ANALYTICAL AND DIAGNOSTICAL STUDIES OF ATOMIC AND IONIC FLUORESCENCE IN THE INDUCTIVELY COUPLED ARGON PLASMA

by

MICHAEL ANTHONY KOSINSKI

A DISSERTATION PRESENTED TO THE GRADUATE COUNCIL
OF THE UNIVERSITY OF FLORIDA IN
PARTIAL FULFILLMENT OF THE REQUIREMENTS
FOR THE DEGREE OF DOCTOR OF PHILOSOPHY

UNIVERSITY OF FLORIDA

1982

To my mother and father, whose loving support made all this possible.

ACKNOWLEDGMENTS

I am grateful to Art Grant, Chester Eastman, and Dailey Burch of the machine shop and Russ Pierce, Walt Johnston and Steve Miles of the electronics shop for their help and construction of some of the instrumentation used in this work.

I also wish to thank Dr. Edward Voigtman and Dr. Benjamin Smith who have helped me enormously during my graduate career. Dr. Voigtman has constructed many of the electronic components referenced in this work such as integrators, photodiode circuits and energy meters and has helped me with the contruction of other electronic components.

Many thanks are extended to Dr. Nicolo Omenetto, with whom I have worked on a few occasions. I have learned much from Nick about laser theory and applications.

Dr. Hiroshi Uchida, with whom I have worked during my last year of graduate study, also deserves many thanks. I am indebted to Hiro for the knowledge I have gained while working with him and for his helping me become a better researcher. His wit and good humor made working long hours in lab more enjoyable. He is

also responsible for drawing all of the figures in this dissertation.

I owe a special debt of gratitude to Dr. James D. Winefordner, my graduate research professor. Without "Doc," none of this could have been accomplished. I am grateful that I was given the opportunity to work in his research group.

Lastly, I must thank Peggy Lee for the many hours spent typing this dissertation.

TABLE OF CONTENTS

page

Abstract of Dissertation Presented to
the Graduate Council of the University of Florida
in Partial Fulfillment of the Requirements
for the Degree of Doctor of Philosophy

ANALYTICAL AND DIAGNOSTICAL STUDIES OF ATOMIC AND IONIC FLUORESCENCE IN THE INDUCTIVELY COUPLED ARGON PLASMA

by

MICHAEL ANTHONY KOSINSKI

December 1982

Chairman: James D. Winefordner
Major Department: Chemistry

The characteristics of atomic and ionic fluorescence excited by a pulsed dye laser in the inductively coupled plasma (ICP) using two different torch designs have been investigated. Vertical distributions of atomic and ionic fluorescence intensities for calcium and yttrium were directly obtained in the central axis of the plasma without the need of an Abel inversion procedure and thermally-assisted fluorescence intensities were found not to follow a Boltzmann distribution. The usefulness of the ICP as an atomization or ionization cell in fluorescence spectrometry is also discussed.

Fluorescence lifetimes provide valuable information concerning quenching processes occurring in different gas compositions. In an ICP, the inert gas atmosphere would seem to provide a high quantum yield for atomic fluorescence studies. The determination of atomic excited-state lifetimes in an ICP was carried out and from the ratio of the observed lifetime to the natural radiative lifetime, quantum efficiencies were calculated for various heights in the ICP for two different torch designs. With the laser system used, single shot fluorescence lifetimes greater than about 4 ns could be measured without any deconvolution of the laser pulse being needed.

The ICP is not only useful as an atomization cell for emission or fluorescence spectrometry. In this work, an ICP was also used as an excitation source for fluorescence measurements in a second ICP. A high concentration of the analyte element was aspirated into the ICP used for excitation while aspirating increasing concentrations of the same element into the ICP used for atomization. Characteristics of the dual ICP configuration, such as vertical distributions of atomic and ionic fluorescence intensities, curves of growth, chemical and spectral interferences and detection powers are discussed.

CHAPTER I
INTRODUCTION

The inductively coupled plasma (ICP) is the best simultaneous multielement atomic emission spectrometry (AES) excitation source for the analysis of major, minor and trace elements in various materials, because of high sensitivities, wide dynamic ranges and freedom from chemical and ionization interferences (1). In spite of these advantages, there are a number of difficulties associated with the use of ICP-AES, notably the occurrence of spectral interferences, the need for careful optimization to minimize multiplicative interferences and the variation in nebulization efficiency caused by variation in solution viscosities (2, 3). Because of the high temperature in the ICP, the spectra are rich in lines and even the use of a high resolving power monochromator does not enable all the analytically useful lines to be used in certain analyses.

In principle, fluorescence techniques, although requiring an intense primary excitation source, should be effective in avoiding spectral interferences. Atomic fluorescence techniques using a xenon arc lamp (4), electrodeless discharge lamps (EDLs) (5), hollow cathode

lamps (HCLs) (6), ICP emission (7) and a pulsed tunable dye laser (8) as primary excitation sources have been reported for flame atomization. Limits of detection (LODs) were improved using laser excitation (9), some of which were equivalent to or better than those in flame atomic absorption spectrometry (AAS) and ICP-AES. However, in a flame, chemical and ionization interferences are often observed and poor detection powers for refractory elements cannot be avoided. These should be improved by using the ICP as an atomization cell, because of its high temperature, high electron number density and relatively long residence time of the analyte. The high volatilization efficiency achieved in the ICP also should minimize the scattering of excitation radiation. Furthermore, quenching effects caused by molecular species should be less compared with combustion flames.

In this work, for the laser-excited ICP technique, an attempt will be made to determine (i) the principle factors affecting fluorescence sensitivities in the ICP; (ii) the existence of thermally-assisted fluorescence in the ICP and the use of this technique for temperature measurements; (iii) the effect of the RF (radio-frequency) power and carrier argon flow rate on fluorescence intensities and excitation temperatures; (iv) the variation of excitation temperatures with increasing observation height in the plasma; (v) the presence of chemical and spectral

interferences; (vi) the magnitude of the quantum efficiency in the ICP and (vii) the best plasma observation regions and torch design for analytical atomic and ionic fluorescence measurements in the ICP.

Finally, the ICP spectral irradiance will be used as an excitation source for fluorescence measurements in a second ICP. In this case, an effort will be made to determine (i) the viability of ICP emission as an excitation source; (ii) the best plasma observation regions for atomic and ionic fluorescence measurements in the ICP using the extended-sleeve torch; (iii) the suitability of detection powers for trace element analysis; (iv) the presence of chemical and spectral interferences and (v) the factors limiting the measurements in this technique.

CHAPTER II
DIAGNOSTICAL STUDIES OF LASER-EXCITED ATOMIC AND IONIC FLUORESCENCE

Introduction

Laser-excited atomic fluorescence spectrometry (LEAFS) is a useful technique for measurement of plasma diagnostics such as the spatial distribution of analyte species and of the temperatures in a small volume. When the data are obtained by emission or absorption techniques, an Abel inversion procedure (10) is applied to convert the lateral values into radially resolved information. However, the Abel inversion technique has some difficulties in practice; precise measurements of the lateral intensity at 20 or more points, the exact locations of the center and the edge of the plasma, the exact symmetry of the plasma and the solution of the integral equation by a computer are required. The fluorescence technique is well-suited to obtain spatially resolved information directly without an Abel inversion procedure (11). Relative spatial profiles of barium ion and atom in the ICP using laser-excited fluorescence have already been reported (12).

The LEAFS technique is also well-suited for the determination of analyte excited-state lifetimes. Lifetimes of sodium atoms in various flame gas compositions have previously been reported (13, 14). The fluorescence lifetimes provide valuable information concerning quenching processes occurring in different gas compositions. The sodium lifetime in an air-acetylene flame, for example, was reported by Russo and Hieftje to be less than 1 ns (14). Fluorescence quenching by flame gas molecules obviously plays a significant role in the short lifetime of sodium as compared to its natural radiative lifetime of 16.2 ns.

The diagnostics that this chapter will deal with are (i) characteristics of atomic and ionic fluorescence; (ii) vertical distributions of atomic and ionic fluorescence intensities; (iii) collisional redistribution of radiatively-excited levels and utilization of the thermally-assisted process for temperature measurements; (iv) horizontal distributions of fluorescence intensities; (v) the effect of the RF power on the excitation temperatures and fluorescence intensities; (vi) vertical distributions of the excitation temperatures and fluorescence intensities; (vii) interelement effects; (viii) spectral interferences and (ix) determination of excited atom lifetimes.

Theoretical Considerations

Types of Fluorescence

Basically, there are five types of atomic fluorescence transitions. Resonance fluorescence results when the same lower and upper levels are involved in the excitation and deexcitation processes. Direct-line fluorescence occurs when the same upper level is involved in the excitation and deexcitation processes. If different upper levels are involved, stepwise-line fluorescence results. Sensitized fluorescence results when one species, called the donor, is excited and transfers its energy to another species, called the acceptor, which then deexcites radiationally. Lastly, multiphoton fluorescence occurs when two or more photons excite a species which then deexcites radiationally.

The fluorescence process is termed Stokes if the energy of excitation is greater than the fluorescence energy. The process is termed anti-Stokes if the fluorescence energy is greater than the excitation energy. If the excitation and fluorescence processes involve only excited levels, this is termed excited-state fluorescence. If the excitation process involves collisional excitation following the radiational excitation, the process is termed thermally-assisted fluorescence.

Temperature Measurement Techniques

The process of thermally-assisted fluorescence consists of measuring the fluorescence from collisionally-excited states after radiative excitation. If the collisional rates are fast enough to allow a new Boltzmann distribution during the laser pulse from the thermally-assisted fluorescence, the temperature in small volumes can be measured (15). A Boltzmann plot can be obtained by plotting ln (B_F λ/gA) versus the energy of the upper levels involved, where B_F is the fluorescence signal, λ is the wavelength of the transition and gA is the multiplicity of the level times the Einstein coefficient of spontaneous emission. The temperature can be calculated from the slope of this distribution which is equal to -1/kT. Furthermore, other than the thermally-assisted fluorescence technique, four other kinds of two-line atomic fluorescence temperature measurement techniques have been reported (16), some of which were successfully applied to the measurements of small volume flame temperatures (17, 18). In each of these cases, a Boltzmann distribution involving either the excited-state after radiational excitation and collisions (thermally-assisted case), or the ground and metastable levels (in the other cases) must be assumed.

Two of these temperature measurement techniques will be considered here. The first is the conventional two-line linear fluorescence method. In this case, it has been shown (19-21) that the ratio of the anti-Stokes to the Stokes direct line fluorescence signals obtained when a thallium solution is aspirated in a flame and excited by a spectral continuum source allows calculation of the flame temperature. If saturation of the optical transition (when the process of stimulated emission balances that of absorption) does not occur, then the flame temperature is given by (11)

$$T = \frac{5040\ V_2}{\log\left(\frac{E_{\lambda_{23}}}{E_{\lambda_{13}}}\right) + 6\ \log\left(\frac{\lambda_{23}}{\lambda_{13}}\right) + \log\left(\frac{E_{F(\lambda_{32})}}{E_{F(\lambda_{31})}}\right)} \qquad (2\text{-}1)$$

where V_2 = excitation energy of the metastable level 2 (eV);

$E_{\lambda_{23}}$ = source spectral irradiance for the the excitation transition 2→3 ($J\ cm^{-2}\ s^{-1}\ nm^{-1}$);

$E_{\lambda_{13}}$ = source spectral irradiance for the excitation transition 1→3 ($J\ cm^{-2}\ s^{-1}\ nm^{-1}$);

λ_{23} = wavelength of the transition 2→3 (nm);

λ_{13} = wavelength of the transition 1→3 (nm);

$E_{F(\lambda_{32})}$ = fluorescence irradiance for the transition 3→2 (J cm^{-2} s^{-1} nm^{-1}); and

$E_{F(\lambda_{31})}$ = fluorescence irradiance for the transition 3→1 (J cm^{-2} s^{-1} nm^{-1}).

The second is the saturation two-line fluorescence method. Assuming that optical saturation can be achieved and that the fluorescence waveform can be temporally resolved and measured with a gated detector having a gate much smaller than the fluorescence waveform, the temperature can be calculated from the following relation (11)

$$\frac{B_{F\ \substack{3\to1\\1\to3}}}{B_{F\ \substack{3\to1\\2\to3}}} = \left(\frac{g_2 + g_3}{g_1 + g_3}\right)\left(\frac{g_1}{g_2}\right) e^{(V_2/kT)} \qquad (2\text{-}2)$$

where $B_{F\ \substack{3\to1\\1\to3}}$ = peak fluorescence signal for the resonance process (J cm^{-2} s^{-1} sr^{-1});

$B_{F\ \substack{3\to1\\2\to3}}$ = peak fluorescence signal for the anti-Stokes process (J cm^{-2} s^{-1} sr^{-1});

g = multiplicity of the level;

V_2 = excitation energy of the metastable level 2 (J):

k = Boltzmann constant (1.380×10^{-23} J/K); and

T = temperature (K).

In this case, the ratio of the resonance to the anti-Stokes fluorescence allows calculation of the temperature. Since the same frequency of fluorescence is involved, no calibration of the optical system (as required for the linear two-line flourescence method) is needed. However, it is necessary that saturation of both excitation processes be accomplished and that fluorescence measurements be done only during the early interval of fluorescence where 2-level saturation is achieved.

Excited Atom Lifetimes

Fluorescence lifetimes provide valuable information concerning quenching processes occurring in different gas compositions. Flame gas molecules play a significant role in the quenching of fluorescence. In an ICP, however, the inert argon atmosphere would seem to provide a high quantum yield for atomic fluorescence studies. With the present laser system, single shot fluorescence lifetimes greater than about 4 ns can be measured without any deconvolution of the laser pulse being needed. Measurements of the actual mean lifetime (τ) of the excited atoms in the ICP provides a way to

determine absolute fluorescence quantum yields by using the relation

$$Y = \tau/\tau_{sp} \qquad (2\text{-}3)$$

where Y = quantum efficiency (dimensionless);

τ = measured lifetime (s); and

$\tau_{sp} = 1/A_{21}$ where A_{21} (s^{-1}) is the Einstein coefficient of spontaneous emission.

If level 2 can combine with other lower levels, then

$$\tau_{sp} = 1/\sum_{j} A_{2j} \qquad (2\text{-}4)$$

When several radiative transitions are possible, then each individual quantum efficiency can be calculated provided that the branching ratios are known (13, 14, 22-25).

It would seem that the smaller the difference there is in energy between levels near to the laser-excited level, more efficient collisions would occur and energy would be more easily transferred to these other levels resulting in a short lifetime, compared to the natural radiative lifetime. It will be shown that, depending on the element and the number of levels near the laser-excited level, the quantum efficiency in the ICP ranges from ~0.1-1.0.

To confirm the results obtained for the quantum efficiency in the ICP, the fluorescence ratio of the two sodium D lines for D_1 (589.592 nm) and D_2 (588.995 nm) excitation was examined. It has been shown by Omenetto et al. (26) that when excitation at the D_2 line is used, the fluorescence ratio of the two lines is

$$R_{13} \simeq 2 + \frac{k_{21}}{k_{32}} + \frac{A_{21}}{k_{32}} \qquad (2\text{-}5)$$

where k_{21} = quenching rate constant (s^{-1});
k_{32} = mixing rate constant (s^{-1}); and
A_{21} = Einstein coefficient of spontaneous emission (s^{-1}).

Therefore, if a high quantum efficiency atomization cell is used, the quenching rate constant and the Einstein coefficient will be small compared to the mixing rate constant and the ratio of the two D lines will approach the limiting value of 2.

Also, it has been shown (26) that when excitation at the D_1 line is used, the ratio of the two lines is

$$R_{12} \simeq \frac{2}{1 + \frac{k_{31}}{k_{32}} + \frac{A_{31}}{k_{32}}} \qquad (2\text{-}6)$$

Again, the ratio for the two D lines will approach 2 if

the mixing rate constant is large compared to the quenching rate constant and Einstein coefficient.

Experimental

Instrumentation

A block diagram of the laser-excited ICP system is shown in Figure 2-1. Organic laser dyes used are listed in Table 2-1.

The nitrogen laser (Molectron Corp. UV-14, Sunnyvale, CA) was operated under the following conditions: 26-28 kV applied high voltage, 50 torr nitrogen pressure in laser channel and 20 Hz repetition rate. The dye laser (Molectron Corp. DL 200), which was pumped by the nitrogen laser, contained six static dye cells in a carousel arrangement. Each cell could hold approximately 2 mL of dye solution which was magnetically stirred during the laser operation. The output of the dye laser had an approximately 3-4 ns pulse width and approximately 1-200 μJ peak power depending on the dye and wavelength. The ICP (Plasma-Therm 1500D, Kresson, NJ) was operated under various RF powers and argon flow rates. These conditions will be outlined in detail later. The fluorescence was imaged on the entrance slit of a 350 mm focal length monochromator (Heath Co. EU-700, Benton Harbor, MI; now GCA Corp., McPherson

Instruments, Acton, MA). The entrance and exit slit widths were 0.5 mm and the slit height was 3 mm. The photomultiplier (Hamamatsu, Inc. R928 or R212UH, Middlesex, NJ) was operated at -1000V (Pacific Precision Instruments HV Supply, Concord, CA) and the output signal connected to the boxcar averager (EG & G, Inc., Princeton Applied Research 162/164, Princeton, NJ) via an amplifier with a gain of 10 (Comlinear Corp. CLC100, Loveland, CO). The photoelectric pulse from the laboratory-constructed photodiode circuit was used as a trigger signal for the boxcar averager. The photomultiplier base was modified for fast response (27). The output from the boxcar was integrated for 10s using a laboratory-constructed integrator and the output displayed on a digital voltmeter (John Fluke Mfg. Co., Inc. 8000A, Seattle, WA). For the temperature measurements, a strip chart recorder (Fisher Scientific Co. 5000, Pittsburgh, PA) was utilized and calibration of the spectral response of the detector system was performed with a standard tungsten lamp (Optronics Laboratories, Inc., Orlando, FL). The ICP operating parameters for the various diagnostical studies follow.

Short torch. The short torch (Plasma-Therm T1.0) was utilized for the study of vertical distributions of relative fluorescence and emission intensities for calcium ion and atom as well as the vertical distributions

of relative excited-state thermally-assisted fluorescence and emission intensities for yttrium ion. For these studies, the RF power of the ICP was 1.0 kW, the plasma support argon flow rate was 15 L min^{-1} and auxiliary argon was not used. A cross-flow nebulizer (Nippon Jarrell-Ash, Kyoto, Japan) with a nebulizing gas pressure of 20 or 30 psig produced argon flow and solution uptake rates of 0.93 and 1.24 L min^{-1} and 1.13 and 1.43 mL min^{-1}, respectively.

Extended-sleeve torch. The extended-sleeve torch (Baird Corp., Bedford, MA) was used for studying horizontal and vertical distributions of atomic and ionic fluorescence intensities, vertical distributions of excitation temperatures, interelement effects and the effect of the RF power on the fluorescence intensities and excitation temperatures.

The RF powers used were 0.7 kW for the atomic lines of calcium, gallium, strontium, thallium and lead and 1.0 kW for the atomic lines of aluminium, molybdenum, vanadium and for all the ionic lines, except for the lines of yttrium and zirconium where 1.2 kW was used. The plasma support argon flow rate was 15 L min^{-1} and auxiliary argon was not used. The cross-flow nebulizer was operated at a pressure of 40 psig which produced argon flow and solution uptake rates of 1.7 L min^{-1} and 2.2 mL min^{-1}, respectively.

Lifetime studies. A block diagram of the experimental system is shown in Figure 2-2. The nitrogen laser, dye laser, laser dyes and laser operating parameters (Molectron Corp.) are the same as previously described. The output of the dye laser was focused to a 3 mm diameter in the central axis of the ICP (Plasma-Therm 1500D) and the resultant fluorescence was observed at a 90 degree angle with a 350 mm focal length monochromator (Heath Co. EU-700). The ICP was operated at 1.0 kW RF power and 15 L min^{-1} plasma support argon flow rate. Auxiliary argon was not used. Both a short torch (Plasma-Therm T1.0) and an extended-sleeve torch (Baird Corp.) were examined. Carrier argon nebulizing pressures were 20 and 40 psig for the short and extended-sleeve torches, respectively. The photomultiplier tube (Hamamatsu, Inc. R928) was operated at -1000V (Pacific Precision Instruments HV Supply) and the base modified for fast response (27). A short length (approximately 50 cm) of RG58U cable was used between the photomultiplier and the 400 MHz input of the storage oscilloscope (Tektronix, Inc. 7834, Beaverton, OR) to avoid distortion of the fluorescence decay curve. The photoelectric pulse from the laboratory-constructed photodiode circuit provided a stable trigger for the oscilloscope. The concentration of the elements used was either 100 or 1000 μg mL^{-1} with care being taken not to saturate the

detector system by checking with neutral density filters and adjusting the slit width of the monochromator.

Chemicals

Stock solutions of 1000 μg mL^{-1} were prepared from the pure metal when possible or from reagent grade chemicals, dissolved in the minimum amount of acid and succesively diluted with distilled/deionized water.

Results and Discussion

Characteristics of Atomic and Ionic Fluorescence Using a Short Torch

Laser-excited atomic fluorescence has been carried out mainly in a flame and few reports of ionic fluorescence have appeared both in flames (11) and ICPs (12, 28, 29). In the analytical region (10-25 mm above the load coil) of the ICP, atoms are largely converted into ions. Consequently, the ICP should be effective as an ionization cell for ionic fluorescence spectrometry.

The relative ionic fluorescence intensities and gA values (30) of yttrium obtained under the conditions of 1.0 kW RF power, 15 L min^{-1} plasma support argon flow rate, 20 psig nebulizing gas pressure and an observation height of 15 mm above the load coil are given in Table 2-2. The laser-excited lines are listed together with dyes and energies, which were roughly measured by a

laboratory-constructed energy meter. A simplified energy-level diagram for the pertinent transitions is shown in Figure 2-3.

Considering the relative fluorescence intensities obtained, the dominant factor which affects the sensitivity seems to be the spontaneous transition probability (Einstein coefficient of spontaneous emission) value of the fluorescence line (31). The second factor appears to be the energy difference of the upper levels between the laser-excited and fluorescence lines. In this regard, the resonance line should be the most sensitive. However, the sensitivity of the Stokes or anti-Stokes fluorescence line (32) sometimes exceeds that of the resonance line; in particular, when the laser energy at the resonance line is weak, as shown for 508.742 nm (excited line)/371.030 nm (fluorescence line). Further, thermally-assisted fluorescence (32) is fairly sensitive when the difference between the upper levels is small, as is shown for 383.288 nm/371.030 nm. Excited-state fluorescence (27) intensities are relatively stronger in the ICP than those in a flame, as a consequence of the increase in the population of the excited lower level because of the higher ICP temperature compared to the flame. Similar results were obtained for the atomic fluorescence of iron and thallium in the ICP.

Vertical Distributions of Atomic and Ionic Fluorescence Intensities Using a Short Torch

The spatial distributions of species densities of the plasma support argon and/or analyte atoms are important for plasma diagnostics (12).

Vertical distributions along the central axis of the plasma, which are difficult to obtain exactly by the Abel inversion procedure because of measurement and calculation errors, contain valuable information about the excitation process in the ICP. Here, vertical distributions of ionic resonance fluorescence, atomic resonance fluorescence and excited-state thermally-assisted fluorescence intensities (32) are presented.

The vertical distributions of fluorescence and emission intensities for calcium ion at 393.367 nm (0-25414 cm^{-1}) at carrier argon flow rates of 0.93 and 1.24 L min^{-1} are shown in Figure 2-4. Significant differences exist in the distributions between fluorescence and emission intensities. At 0.93 L min^{-1} flow rate, maximum emission exists at 10 mm above the load coil and that of fluorescence at 20 mm. When the carrier argon flow rate increases from 0.93 to 1.24 L min^{-1}, the fluorescence intensity increases and the maximum fluorescence (peak) is slightly shifted to a higher position. These phenomena are mainly due to the increase of the transport rate of calcium into the

plasma and of the ground-state population with the decrease in temperature. The latter is confirmed by the decrease in emission intensity with increase of carrier flow rate (33).

The vertical distributions of fluorescence and emission intensities for calcium atom at 422.673 nm (0-23652 cm^{-1}) at the same two carrier argon flow rates are shown in Figure 2-5. Again, the fluorescence distribution reflects the population density of the calcium atom ground-state. Here, a more rapid decrease in emission and fluorescence intensities with increase in observation height is observed at both carrier argon flow rates as compared with calcium ion. The increase of the fluorescence intensity at the higher carrier gas flow rate (1.24 L min^{-1} compared to 0.93 L min^{-1}) is caused by an increase in the total calcium number density resulting from an increase in the calcium transport rate and by the increase in the ground-state population with the decrease in temperature. Furthermore, the emission intensity decreases and its distribution shifts to a higher position with the increase in carrier gas flow rate.

The distributions for yttrium ion fluorescence at 371.030 nm (1450-28394 cm^{-1}) are given in Figure 2-6. The fluorescence was obtained by the thermally-assisted process (32) after laser excitation at 383.288 nm

(1450-17532 cm^{-1}). At the higher sample introduction rate corresponding to 1.24 L min^{-1} carrier argon flow rate, the fluorescence intensity decreased in the region of 10-20 mm above the load coil, similar to the emission at 371.030 nm. The decrease in fluorescence is probably due to the decrease in population of the excited lower state (1450 cm^{-1}) and the decrease of the thermal collision rate of the analyte (mixing of the 27537 and 28394 cm^{-1} levels).

Collisional Redistribution of Radiatively-Excited Levels and Utilization of the Thermally-Assisted Process for Temperature Measurements Using a Short Torch

A Boltzmann plot resulting from the measurements of yttrium emission intensity (see Figure 2-7) is linear, although some points which varied widely from the line were omitted. These disparate points might have been due to systematic errors in the reported gA values (30). The excitation temperature of yttrium ion, calculated from the slope (34), is 4630K.

A plot of the redistribution of thermally-assisted fluorescence for yttrium using laser excitation at 383.288 nm is shown in the lower part of Figure 2-7. This wavelength was chosen for laser excitation because of the higher laser output power compared to other laser-excited lines (see Table 2-2). The transitions measured were at the same wavelengths used for the emission

measurements. The greater the energy difference between the laser-excited level and the upper states of the fluorescence lines, the greater the deviation from the line, which would be drawn assuming a Boltzmann distribution. The shape of the plot seems to be symmetrical, but the fluorescence intensities in low excited levels (23000-25000 cm^{-1}) could not be detected because of their small gA values. Similar plots were obtained in the ICP for the atomic fluorescence of iron and thallium. The maximum value of the energy difference for which thermally-assisted fluorescence can be observed is about 1.2 eV even if the spontaneous transition probability of the thermally-assisted level is high. This is quite different compared to flames for which the fluorescence of levels as high as ~2 eV above the laser-excited level could be observed.

In a combustion flame, in which the existence of local thermal equilibrium (LTE) is expected, collisional redistribution of radiatively-excited levels (Boltzmann law) has been achieved. For gallium and thallium in an O_2-C_2H_2-Ar flame (35), the levels above the laser-excited level were found to follow a Boltzmann distribution. The slope of this distribution (equal to -1/kT) provided an excitation temperature. The technique using thermally-assisted fluorescence has been established for small-volume temperature measurements in a flame (15,

16, 35). However, the laser-excited level was found to be slightly overpopulated. On the other hand, the level below the laser-excited level was underpopulated with respect to the Boltzmann equilibrium.

Two kinds of two-line fluorescence temperature measurement methods (linear and saturation with sequential pumping at Y(II) 371.030 nm and Y(II) 508.742 nm were carried out in the ICP. The saturation two-line method gave erroneously high temperature values whereas the linear two-line method appeared to give reasonable values.

One of the differences in the characteristics between combustion flames and the ICP is the existence of major molecular species in a flame, such as CO, CO_2, N_2, etc. Since atoms in a flame are excited and de-excited by collisions with molecular species, a decrease of mean lifetimes results, compared with the natural radiative lifetime (13). Laser-excited atoms are thermally redistributed by collisions with molecular species. On the other hand, the ICP is not in complete LTE, which has been confirmed from temperature calculations (10, 34, 36-41). The populations of plasma support gas and analyte species are each described by a Boltzmann distribution, but with different temperatures. However, for laser excitation in the ICP, the radiatively-excited level is overpopulated and the other levels do not follow a Boltzmann distribution with a reasonable

temperature for the negative slope points (see Figure 2-7). A temperature of ~2000K was obtained when a temperature of ~5000K could be expected. A significant difference appears to exist in the excitation mechanisms between radiatively (laser) and non-radiatively excited atoms.

Horizontal Distributions of Fluorescence Intensities Using an Extended-Sleeve Torch

In Figure 2-8, the horizontal distributions of ionic fluorescence intensities for Ca(II) at 393.4/393.4 nm (indicated as excitation λ/fluorescence λ) at three heights are shown. The heights of 5, 15 and 25 mm above the top of the extended-sleeve torch correspond to 45, 55 and 65 mm above the load coil, respectively, since the outer sleeve of the torch extends for 40 mm beyond the top of the load coil. In this experiment, the diameter of the dye laser at the ICP position was about 3 mm and the width and height of the monochromator slits were 0.5 mm and 3 mm, respectively.

These distributions indicate the spatially resolved relative number densities for calcium ion above the top of the extended-sleeve torch. Every distribution has a symmetrical profile and the peak maximum is located in the central axis of the plasma. The fluorescence intensity decreases and the distribution profile becomes slightly wider with an increase in

observation height. Comparing these distributions to those obtained with a conventional short torch, however, the extended-sleeve torch is fairly effective in preventing analyte diffusion into the surrounding air.

Effect of the RF Power on the Excitation Temperatures and Fluorescence Intensities Using an Extended-Sleeve Torch

The RF power of the ICP is one of the significant parameters affecting plasma temperature and fluorescence intensity. An excitation temperature is easily obtained from relative emission intensities and often used for the discussion of plasma diagnostics (10, 33, 40, 41). In Figure 2-9, the effect of the RF power on the iron excitation temperatures at 5 mm above the top of the extended-sleeve torch (45 mm above the load coil) is shown. The temperatures were obtained from a three-line slope calculation using iron atomic emission lines at 382.0, 382.4 and 382.6 nm. Spectral data with respect to these lines have been summarized previously (33). As is shown in Figure 2-9, the temperature increases with increase in RF power and is close to that of a combustion flame. The excitation temperature using the same iron lines and spectral data was found to be 4500K under the conditions of 1.0 kW RF power, 22 psig nebulizing pressure and 20 mm observation height above the load coil with a conventional short torch.

In Figure 2-10, the effect of the RF power on the fluorescence intensities for Ga(I) at 403.3/403.3 nm, Mo(I) at 386.4/386.4 nm, Ca(II) at 393.4/393.4 nm and Y(II) at 508.7/371.0 nm at a 5 mm height above the top of the extended-sleeve torch (45 mm above the load coil) is shown. The intensity of the gallium atomic line (a non-refractory element) decreases with increase in RF power. As can be seen from Figure 2-10, an even lower temperature might be optimal for gallium. However, RF powers below 0.7 kW were not investigated. The molybdenum atomic line (a refractory element) indicates a maximum fluorescence peak at 1.0 kW (3500K) and calcium ionic fluorescence at about 0.9 kW (3300K). Similar results were obtained for resonance ionic fluorescence for barium at 455.4 nm and for strontium at 407.8 and 421.6 nm.

In contrast, yttrium ionic fluorescence at 508.7/371.0 nm (excited-state anti-Stokes type) should be measured at high power, as is shown in Figure 2-10. One of the reasons for the yttrium results might be that the lower level of the laser excitation at 508.7 nm is fairly high above the ground-state (8743 cm^{-1}). However, similar results were also obtained for other yttrium ionic lines, involving the resonance line excited from the ground-state at 363.3 nm and also for Zn(II) 431.7/349.6 nm.

Vertical Distributions of the Excitation Temperatures and Fluorescence Intensities Using an Extended-Sleeve Torch

Vertical distributions of the iron excitation temperatures at 0.7 kW and 1.0 kW RF powers in the central axis of the ICP are shown in Figure 2-11. An Abel inversion procedure was not carried out at each iron emission intensity. For both powers, the temperature decreases at the higher observation points. At 0.7 kW, the temperature is almost equal to that of a N_2O-C_2H_2 combustion flame, especially at the higher positions.

The vertical distributions of fluorescence intensities along the central axis of the plasma for Ga(I) 403.3/403.3 nm (0.7 kW), Ca(II) 383.4/393.4 nm (1.0 kW) and Mo(I) 386.4/386.4 nm (1.0 kW) are shown in Figure 2-12. All three elements are affected by lateral diffusion to the same extent, but in the case of calcium, the decreasing temperature (see Figure 2-11) would result in a depopulation of the first ionic state. Furthermore, because of the formation of monoxides, the molybdenum fluorescence intensity decreases even more.

The background intensity level at 5 mm above the top of the extended-sleeve torch was slightly larger than that at higher positions. However, the noise level was almost the same at all heights examined with this torch.

Interelement Effects Using an Extended-Sleeve Torch

In low temperature combustion flames, the presence of phosphorus sometimes reduces the absorption or fluorescence signal intensity because of the formation of refractory compounds. In Figure 2-13, the effect of the presence of phosphorus on calcium ionic fluorescence intensity is shown. The intensity was slightly suppressed by the presence of phosphorus, being primarily due to the increase in sample solution viscosity (2, 3). A similar result was obtained at 0.7 kW RF power.

The effect of the presence of aluminum on calcium ionic fluorescence intensity at 0.7 kW and 1.0 kW RF power is also shown in Figure 2-13. At 0.7 kW RF power, the fluorescence intensity decreased with an increase in aluminum concentration possibly because of the refractory compound formation of calcium and aluminum in the solute vaporization process. This formation might occur to a lesser extent at higher temperatures, as is shown at 1.0 kW RF power.

The effect of the presence of sodium on the calcium ionic fluorescence intensity is shown in Figure 2-14. The results are quite complicated. At 0.7 kW, calcium ionic fluorescence intensity decreases rapidly with increase in sodium concentration, which seems to be due to an ionization interference. In contrast, the intensity profiles have a peak in the presence of

100 μg mL^{-1} sodium at 1.0 and 1.2 kW RF power possibly due to a change in the atom and ion distributions in the plasma (42). Similar enhancements were observed at higher carrier argon flow rates (>1.0 L min^{-1}) at 15 mm above the load coil with a conventional short torch in the ICP (33). The signal suppression at high concentrations of sodium is also primarily due to the sample solution viscosity (2, 3).

In Figure 2-15, the effect of the presence of sodium on lead atomic fluorescence intensity is shown. It can be seen that at 0.7 kW RF power, there is not much of an interference. However, at 1.0 and 1.2 kW RF power, there is a sharp increase in the lead fluorescence intensity and is due to an ionization interference. The effect, though, is less pronounced at 1.2 kW possibly being due in part to ionization of lead in the higher temperature plasma. The signal suppression at high concentrations of sodium is mostly due to the increase in sample solution viscosity (2, 3).

Spectral Interferences Using an Extended-Sleeve Torch

One of the major disadvantages in the ICP-AES method is spectral interference, namely, the change of background emission caused by stray light and overlapping of the emission spectra. The fluorescence technique should be considerably less susceptible to

spectral interferences since multiple excitation is minimized because the laser excitation line is only 0.03 nm wide (43), and spectral interferences in the resultant spectra are greatly reduced because fluorescence spectra contain fewer lines than those produced by collisional excitation.

The fluorescence excitation and emission spectra (~370-372 nm) for a 100 μg mL^{-1} yttrium solution containing a 5000 μg mL^{-1} iron matrix are shown in Figure 2-16. Emission measurements were carried out under the conditions of 1.0 kW RF power, 20 psig nebulizing gas pressure and 15 mm observation height above the load coil using a conventional short torch. Further, the monochromator grating was scanned with entrance and exit slit widths of 0.02 mm (spectral bandpass = 0.04 nm). On the contrary, fluorescence excitation profiles, using an extended-sleeve torch, were obtained by scanning the dye laser grating at a fixed monochromator wavelength with 1 mm slit widths (spectral bandpass = 2 nm). The dye laser (PBD dye) was optimized at 371.0 nm. Even with the 50 times greater bandpass, the spectral profile for fluorescence shows no overlap between the Y(II) 371.030 nm line and the Fe(I) 370.925 nm line as compared to the emission spectra as shown in Figure 2-16.

Determination of Excited Atom Lifetimes

In Figure 2-17, a typical fluorescence decay curve for sodium along with the dye laser pulse is shown. The full width at half-maximum (FWHM) of the laser pulse was found to be 3.5-4.0 ns with a decay time of 2.0-3.0 ns, which agrees well with the values obtained from streak camera measurements by Zizak et al. (35). In Table 2-3, the experimentally observed lifetimes and calculated quantum efficiences are given for the resonance atomic transitions of 5 elements, together with the radiative lifetime (τ_{sp}). This last figure can be obtained using the known transition probabilities for the different lines originating from the excited levels (22, 35, 44, 45). The measurements were taken at a 10 mm height above the load coil for the short torch and at a 45 mm height above the load coil (5 mm above the top of the torch) for the extended-sleeve torch. As can be seen from Table 2-3, the overall quantum efficiency (τ/τ_{sp}) of the excited atomic levels investigated is very high. This seems to indicate that, at least in the case of neutral atomic "soft" lines (46), electron quenching does not occur to a significant extent.

A change in the RF power from 0.7 to 1.2 kW and in the nebulizing gas pressure from 20 to 40 psig did

not result in an observable change of the lifetimes, which remained the same within experimental error.

In order to see the effect of air entrainment (i.e. increased quenching) when the observation height above the load coil increases, several measurements were performed with sodium at various heights with the two torches available. The resulting variation in lifetimes and calculated quantum efficiencies are shown in Figure 2-18.

It can be seen that entrainment of air in the plasma has a significant effect on the quenching of sodium fluorescence and hence the quantum efficiency, with the conventional short torch. At a height of 25 mm above the load coil, the quantum efficiency has already decreased to about 0.5. However, with the extended-sleeve torch, the quantum efficiency does not drop off to 0.5 until a height of 100 mm above the load coil. This would correspond to 60 mm above the top of the torch since the outer sleeve of the torch extends for 40 mm beyond the top of the load coil. Also, with the extended-sleeve torch, at a height of 80-90 mm above the load coil, the quantum efficiency is still very high (0.85-0.80) even though the plasma has entrained air for a distance of 40-50 mm.

The ratio of the two sodium D lines was experimentally observed in the ICP using a conventional short

torch at a height of 10 mm above the load coil. The ratio in both cases (using D_1 and D_2 excitation) was found to be 2, indicating that the quantum efficiency in the ICP is high and confirming the results obtained for the lifetime measurements. The lifetimes of Fe(I) at 372.0 nm and Y(II) at 383.3 nm were also measured. The lifetime of Fe(I) was about 5 ns and that of Y(II) was close to the limit of the detector response of 4 ns. Even though with the present system an accurate lifetime for Y(II) could not be obtained, it can be safely said to be under 4 ns. Since the natural radiative lifetime for Fe(I) is 61 ns and that for Y(II) is 13.9 ns, a quantum efficiency below 0.2 can be estimated for these elements. As was confirmed from the lifetime measurements of sodium and the ratio of the two sodium D lines, the quantum efficiency in the ICP is high. Therefore, the short lifetimes (compared to the natural radiative lifetimes) of iron and yttrium may be due to quenching by collisional mixing of other levels near the radiatively-excited level with other plasma gas species.

Conclusions

Significant differences exist in the characteristics in laser-excited fluorescence spectra between flames and plasmas. Ionic and excited-state fluorescence are strongly observed in the ICP, and the spontaneous

transition probability value of the fluorescence line is a dominant factor affecting the sensitivity. The LEAFS technique is useful for ICP diagnostics, such as measuring vertical distributions of analyte atoms and ions along the central axis of the plasma. Laser-excited analyte species do not follow a Boltzmann distribution and thermally-assisted collisions are observed only within 1.2 eV of the radiatively-excited level.

The use of the ICP with an extended-sleeve torch was evaluated as an atomization/ionization cell for laser-excited fluoresence spectrometry. Carrier argon flow rate, RF power, observation height and dye laser beam diameter were optimized and excitation temperatures were measured. The temperature of the ICP using this torch was found to be lower than when a conventional short torch is used. Operating parameters, such as RF power and carrier argon flow rate, should be optimized to reduce interelement effects. Also, relative freedom from spectral interferences was found in laser-excited ICP-AFS. From the results obtained in the determination of excited atom lifetimes, it can be concluded that analytical studies in the ICP should be carried out utilizing the extended-sleeve torch for most elements. Use of this torch resulted in a high quantum yield and resistance to quenching by entrainment of air in the plasma. Also, the ability to look high above the load

coil where the temperature is lower and still obtain a large fluorescence quantum yield is achievable with this torch. However, excited-state fluorescence studies might be better performed with a conventional short torch due to its higher temperature of excitation.

Finally, the lifetime measurements can be summarized in the following manner: (i) for the group I elements investigated (Na, Li) that do not have many energy levels near the laser-excited level, the quantum efficiency is close to 1.0; (ii) for the group III elements (Al, Ga, Tl) that have some energy levels near the laser-excited level, the quantum efficiency is $\gtrsim 0.7$; and (iii) for elements such as Fe and Y with many levels close to the laser-excited level, the quantum efficiency is $\lesssim 0.2$.

Table 2-1. List of Laser Dyes Used[1]

Dye	Concentration (Mol L^{-1})	Solvent	Wavelength Peak, nm	Wavelength range, nm (10% points)
PBD	5×10^{-3}	toluene/ethanol 50/50	366, 378	360-386
BBQ	2.5×10^{-3}	toluene/ethanol 50/50	386	373-399
DPS	saturated < 1.2×10^{-3}	p-dioxane	406	396-416
Bis-MSB	1.2×10^{-3}	p-dioxane	421	411-430
C120	5×10^{-3}	ethanol	437	420-457
7D4MC	10^{-2}	ethanol	457	440-478
C500	10^{-2}	ethanol	400	473-547
C495	10^{-2}	ethanol	536	515-583
R6G	5×10^{-3}	ethanol	579	568-605
R6G + CVP	2.5×10^{-3} 3.3×10^{-3}	ethanol	660	641-605

[1]From "Molectron Dye List" by Molectron Corp., Sunnyvale, CA

Table 2-2. Relative Ionic Fluorescence Intensity of Yttrium[1]

	Laser excited wavelength (nm)	363.312	371.063	383.288	508.742	566.294
	Dye Used	PBD	PBD	BBQ	C500	C495
	Laser Energy (μJ/pulse)	20	10	140	50	15
Fluorescence Wavelength (nm)	gA (10^8/sec)	Relative Fluorescence Intensity[2]				
324.228	7.0[3]	70	620	1200	530	970
354.901	2.0	71	720	1800	570	260
363.312	2.6	1900	4100	11000	1700	68
371.030	5.0	1500	16000	17000	26000	160
383.288	1.3	87	1100	9600	1000	23
508.742	0.35	--	3000	1400	2100	30
566.294	1.0	--	190	380	--	2100

[1]Conventional short torch used.

[2]Spectral responses at each wavelength were corrected by using the standard tungsten lamp to calibrate the spectrometer-detector measurement system. The units are arbitrary, but relative to each other.

[3]Reported by Corliss and Bozman (30).

Table 2-3. Experimentally Measured Lifetimes[1]

Species	Excited Transition (wavelength, nm)	τ_{sp}[2] (ns)	Measured τ (ns)		Calculated Quantum Efficiency (τ/τ_{sp})	
			short torch[3]	extended-sleeve torch[4]	short torch	extended-sleeve torch
Al(I)	$^2P_{1/2} \rightarrow {}^2S_{1/2}$ (394.4)	6.8	--	5.1	--	0.76
Ga(I)	$^2P_{1/2} \rightarrow {}^2S_{1/2}$ (403.3)	7.0	5.0	4.8	0.71	0.69
Li(I)	$^2S_{1/2} \rightarrow {}^2P_{1/2,\ 3/2}$ (670.8)	27	24	--	0.89	--
Na(I)	$^2S_{1/2} \rightarrow {}^2P_{1/2,\ 3/2}$ (589.0)	16.2	16	16	0.99	0.99
Tl(I)	$^2P_{1/2} \rightarrow {}^2S_{1/2}$ (377.6)	7.8	5.6	5.5	0.72	0.71

[1]The average lifetimes were obtained from six determinations. Precision (one standard deviation) is approximately 10%.

[2]Values taken from References 22, 35, 44, and 45.

[3]10 mm observation height above load coil.

[4]5 mm observation height above top of the torch (45 mm above load coil).

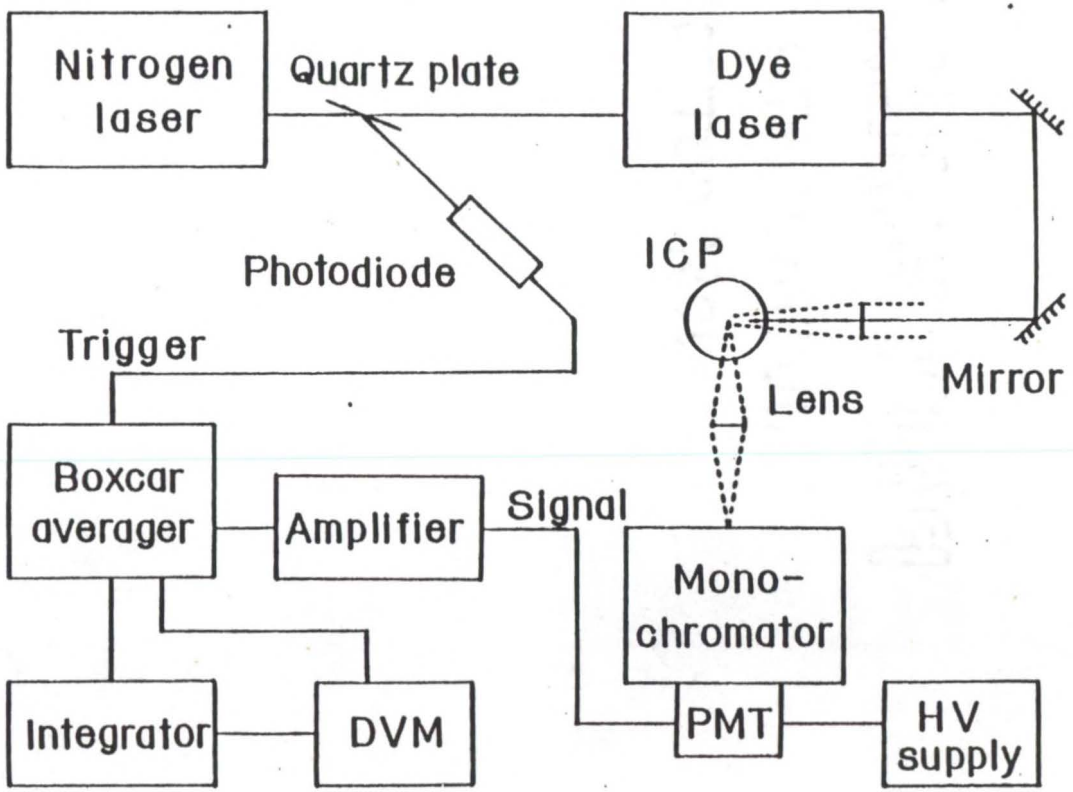

Figure 2-1. Block diagram of laser-excited ICP-AFS system.

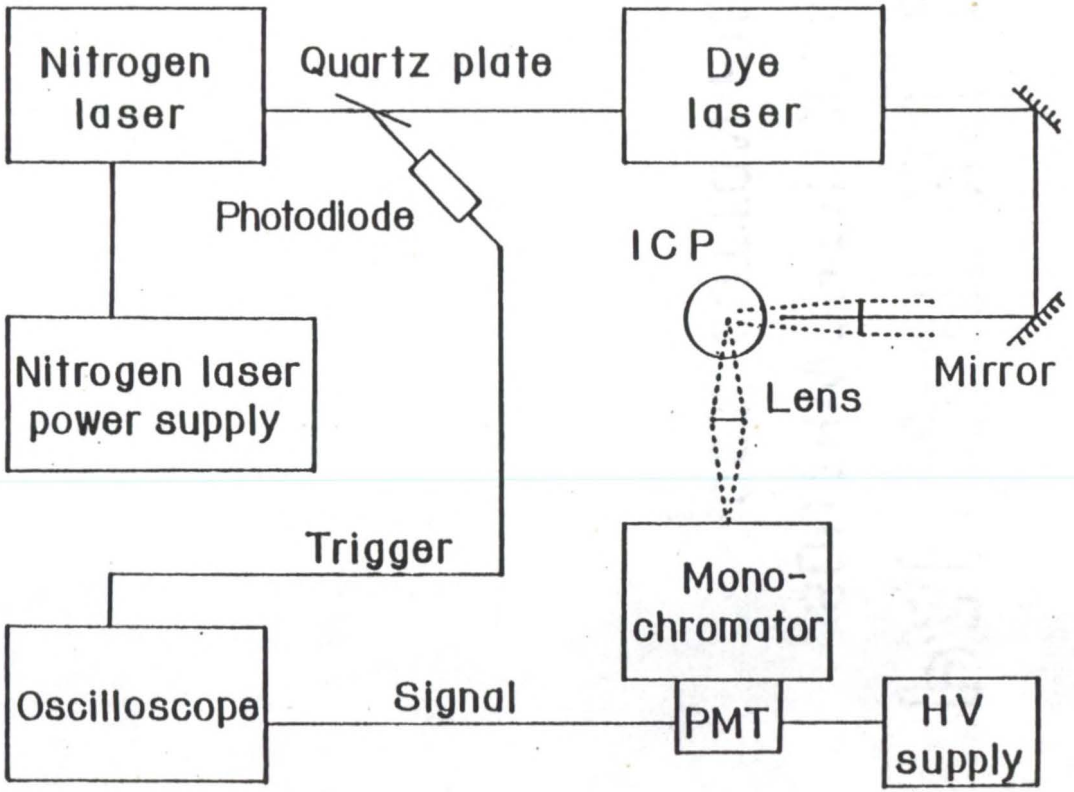

Figure 2-2. Block diagram of laser-excited ICP lifetime measurement system.

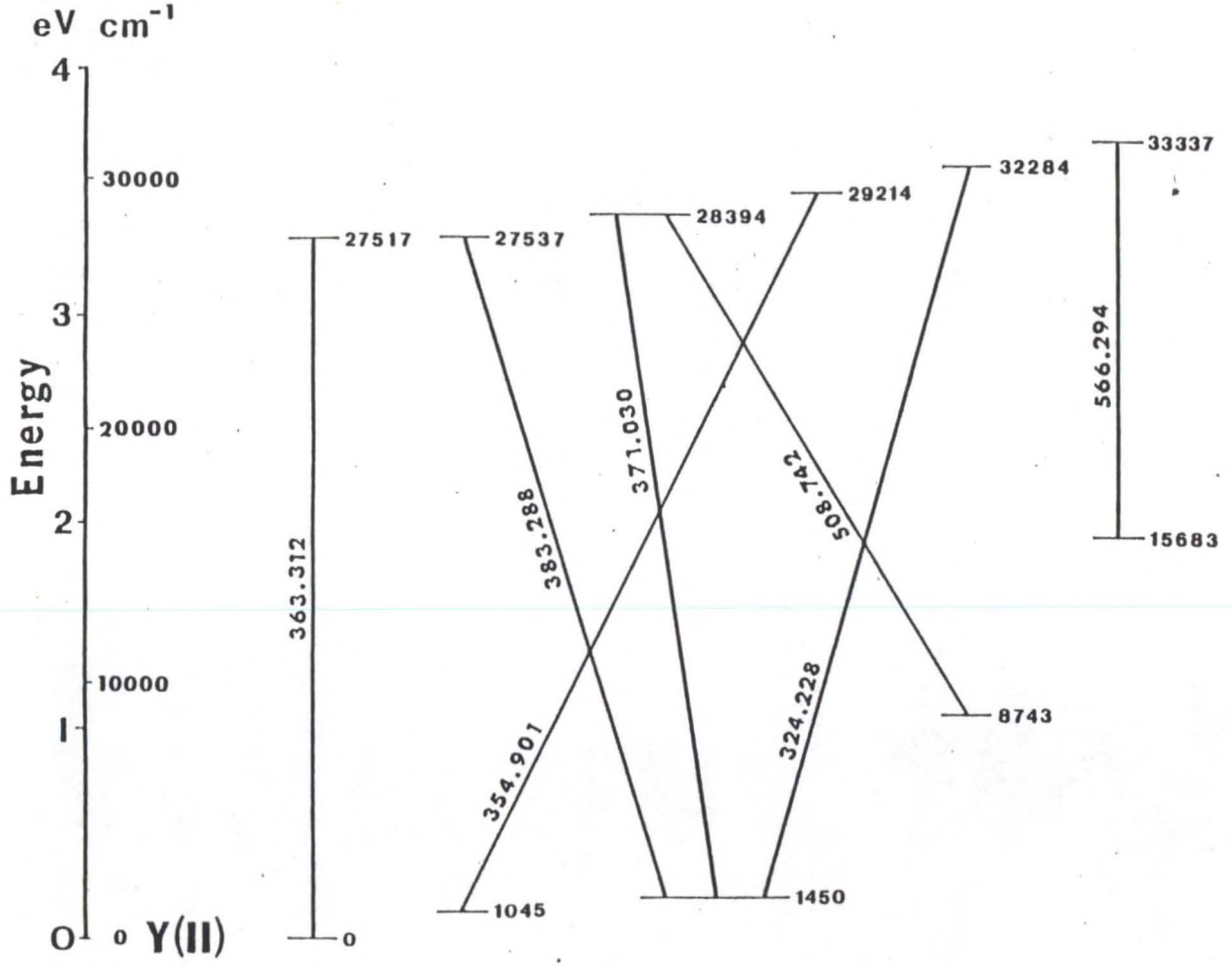

Figure 2-3. Simplified yttrium ion energy-level diagram.

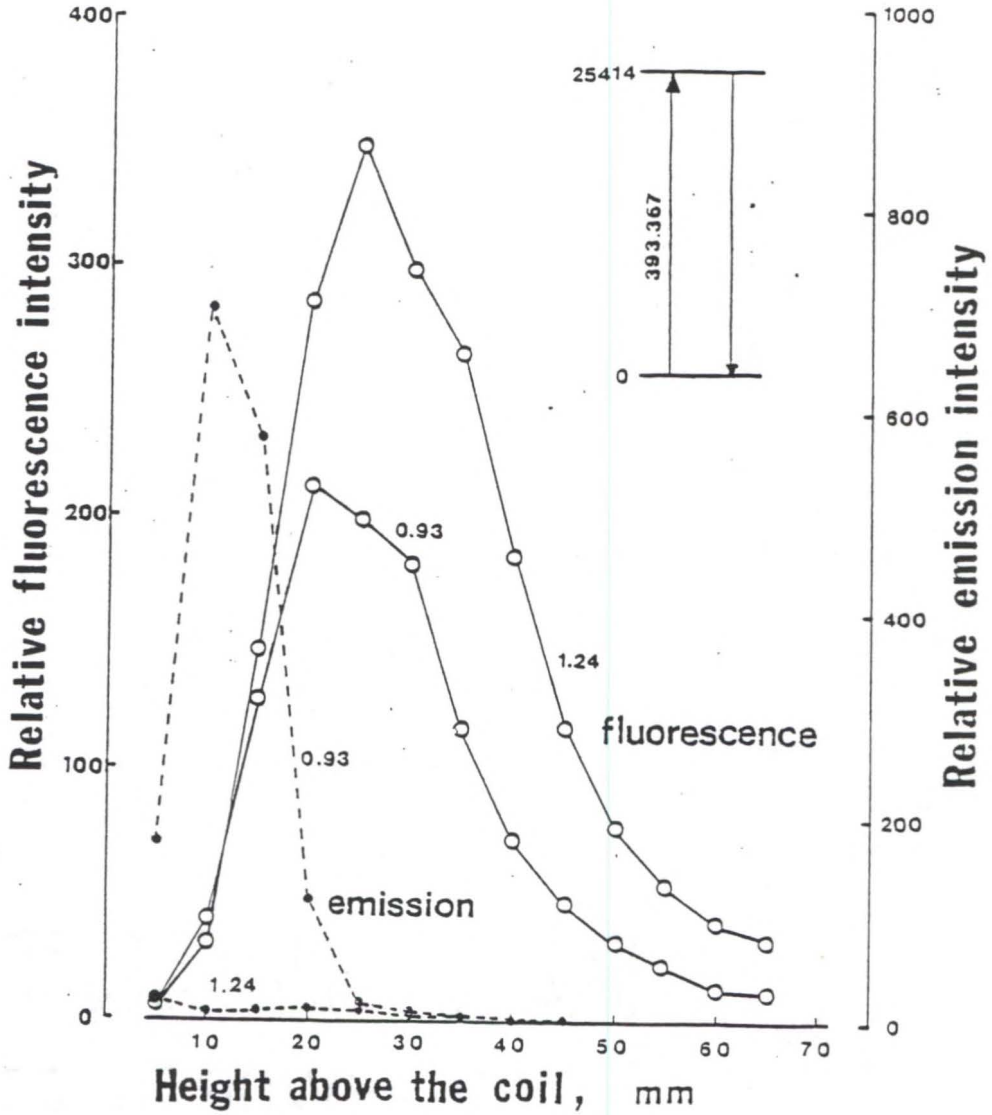

Figure 2-4. Vertical distributions of relative resonance fluorescence and emission intensities for calcium ion at 393.4 nm along the central axis of the plasma. Carrier argon flow rates: 0.93 and 1.24 L/min. Conventional short torch used.

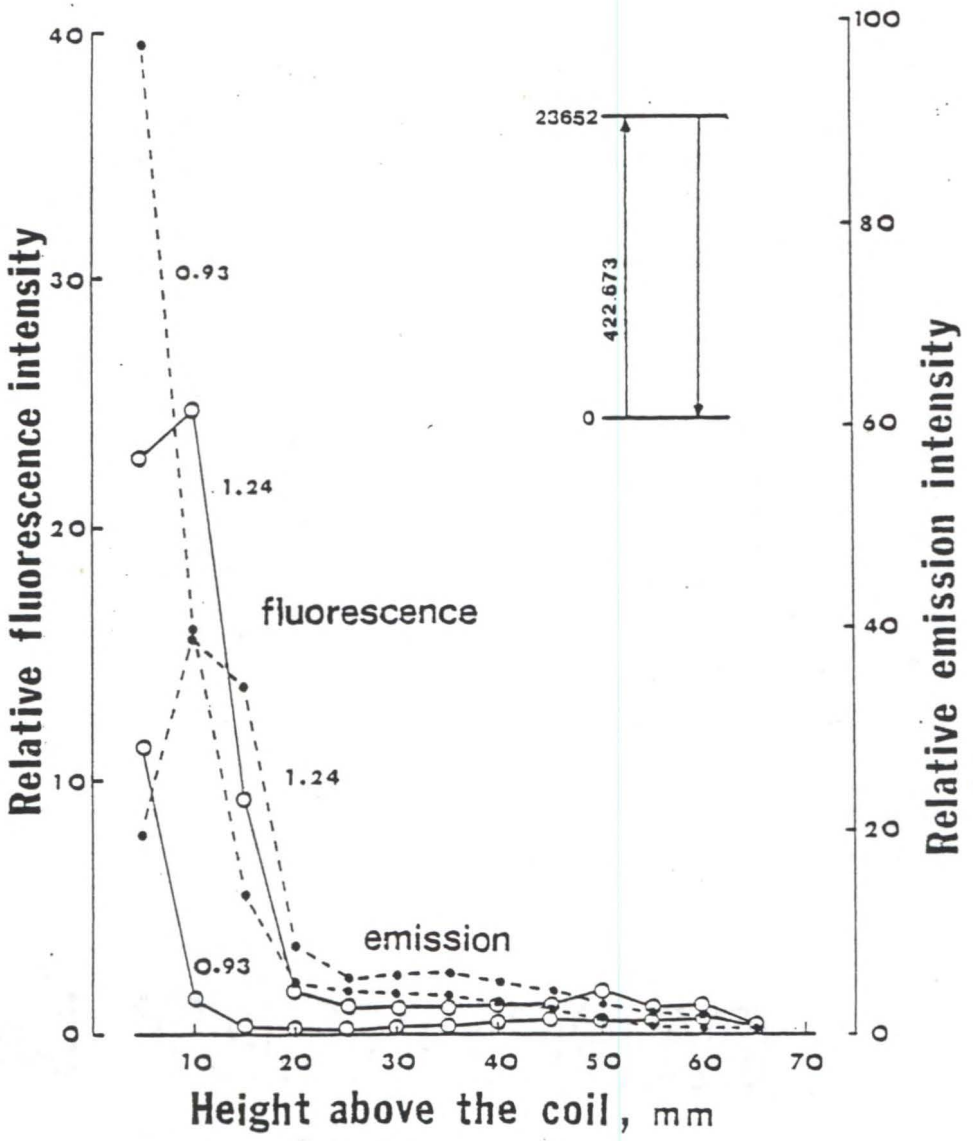

Figure 2-5. Vertical distributions of relative resonance fluorescence and emission intensities for calcium atom at 422.7 nm along the central axis of the plasma. Carrier argon flow rates: 0.93 and 1.24 L/min. Conventional short torch used.

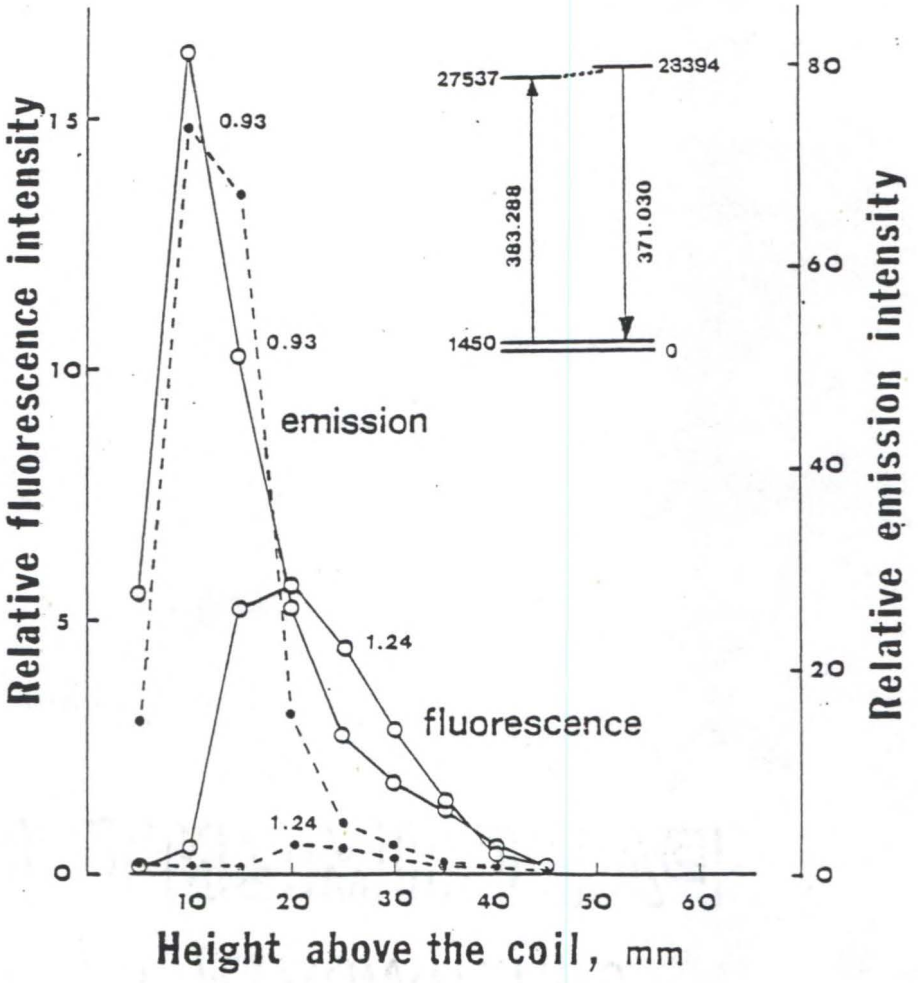

Figure 2-6. Vertical distributions of relative excited-state thermally-assisted fluorescence (excitation wavelength at 383.3 nm) and emission intensities for yttrium ion at 371.0 nm along the central axis of the plasma. Carrier argon flow rates: 0.93 and 1.24 L/min. Conventional short torch used.

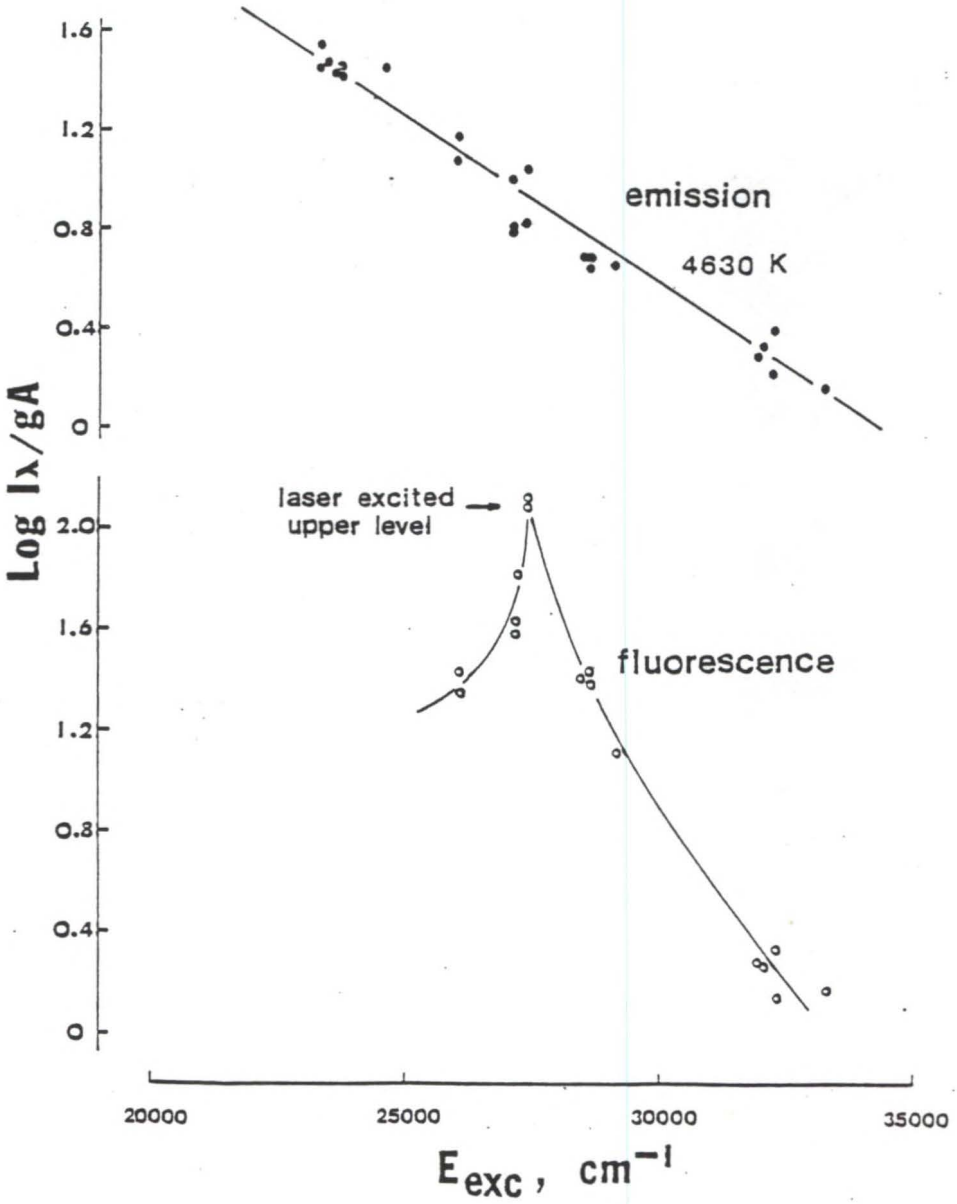

Figure 2-7. Boltzmann plots of emission and thermally-assisted fluorescence (excitation wavelength at 383.3 nm) intensities for yttrium. Carrier argon flow rate: 0.93 L/min. Observation height: 15 mm above the load coil. Conventional short torch used.

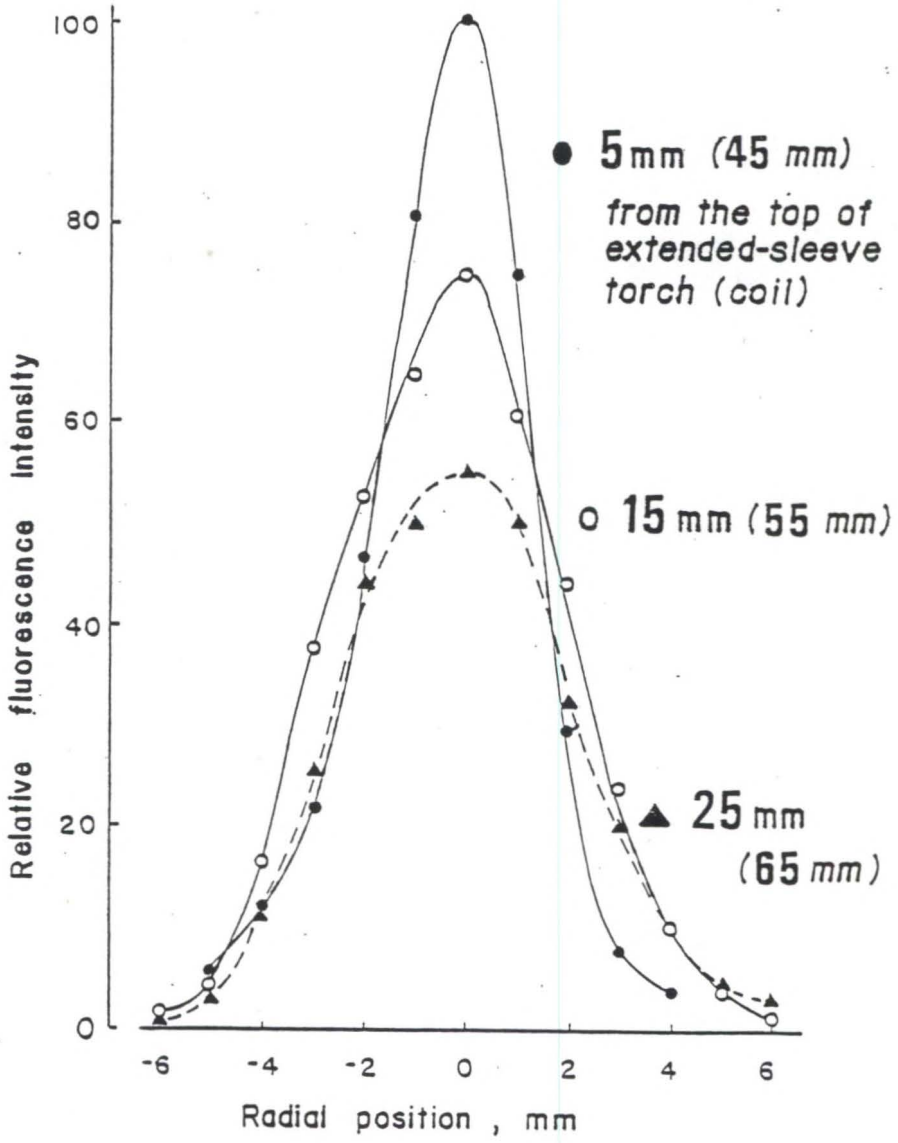

Figure 2-8. Horizontal distributions of resonance fluorescence intensities for calcium ion at 393.4 nm at 5, 15 and 25 mm above the top of the extended-sleeve torch (45, 55 and 65 mm above the load coil). RF power: 1.0 kW.

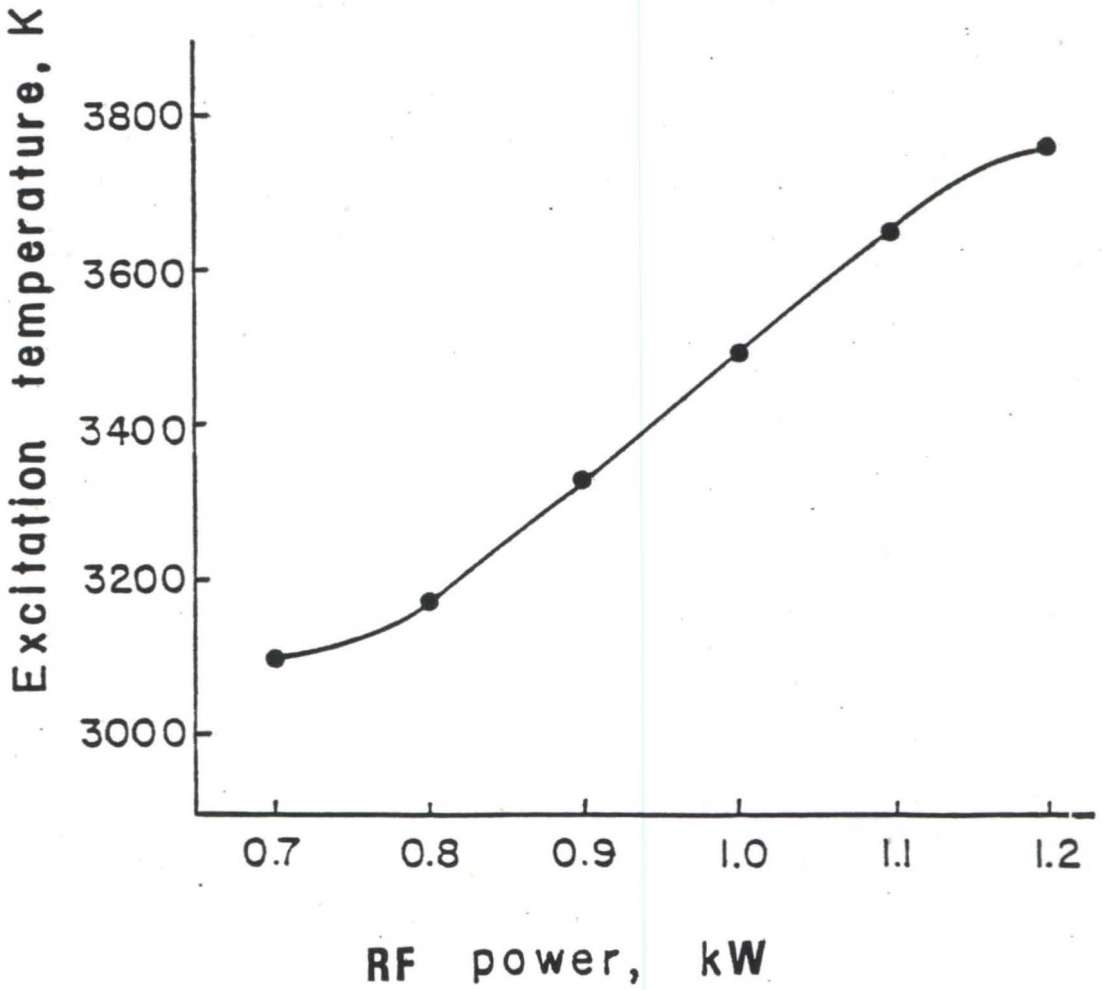

Figure 2-9. Effect of RF power on excitation temperatures. Observation height: 5 mm above the top of the extended-sleeve torch (45 mm above the load coil).

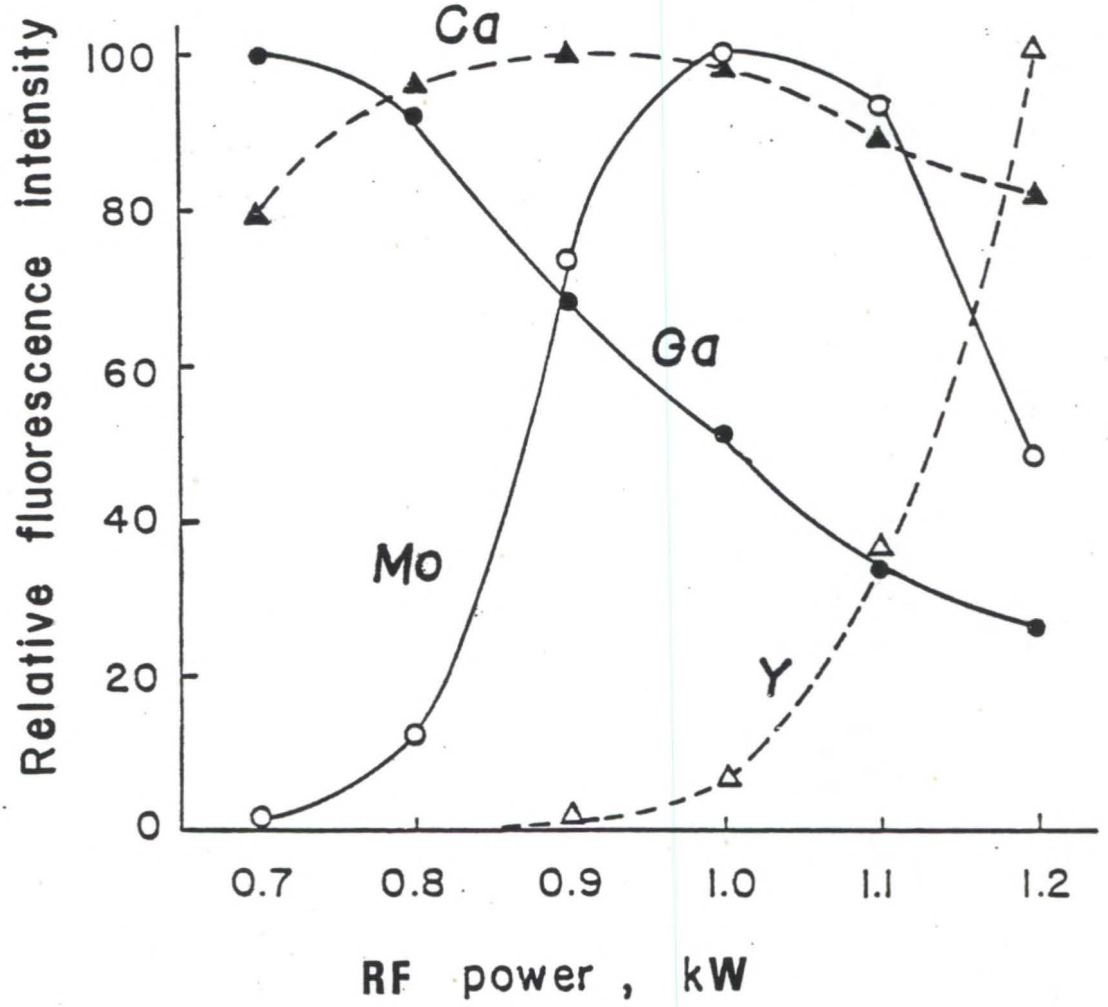

Figure 2-10. Effect of RF power on fluorescence intensities. Observation height: 5 mm above the top of the extended-sleeve torch (45 mm above the load coil). Fluorescence lines: Ga(I) 403.3/403.3 nm, Mo(I) 386.4/386.4 nm, Ca(II) 393.4/393.4 nm, Y(II) 508.7/371.0 nm.

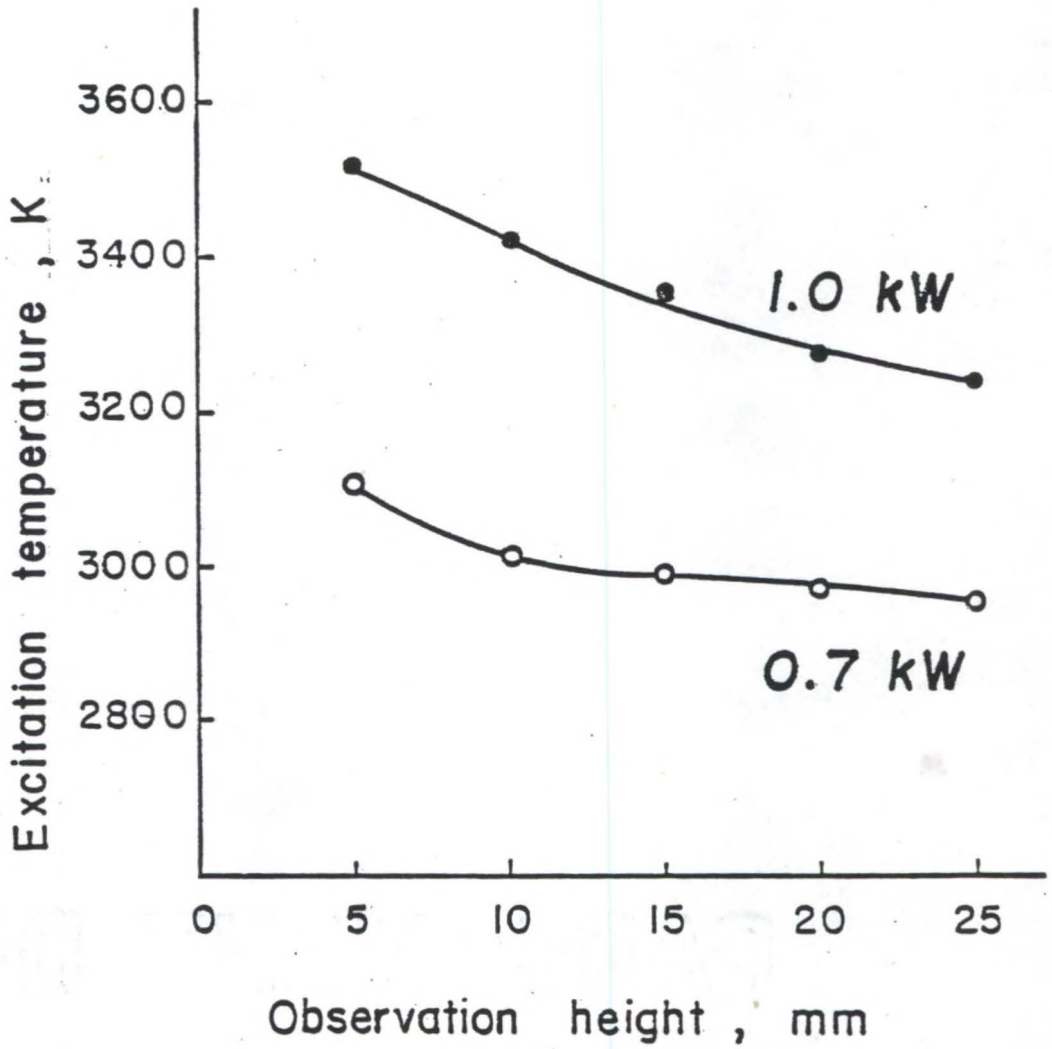

Figure 2-11. Vertical distributions of excitation temperatures. Extended-sleeve torch used. (Observation height is position above the top of the extended-sleeve torch.)

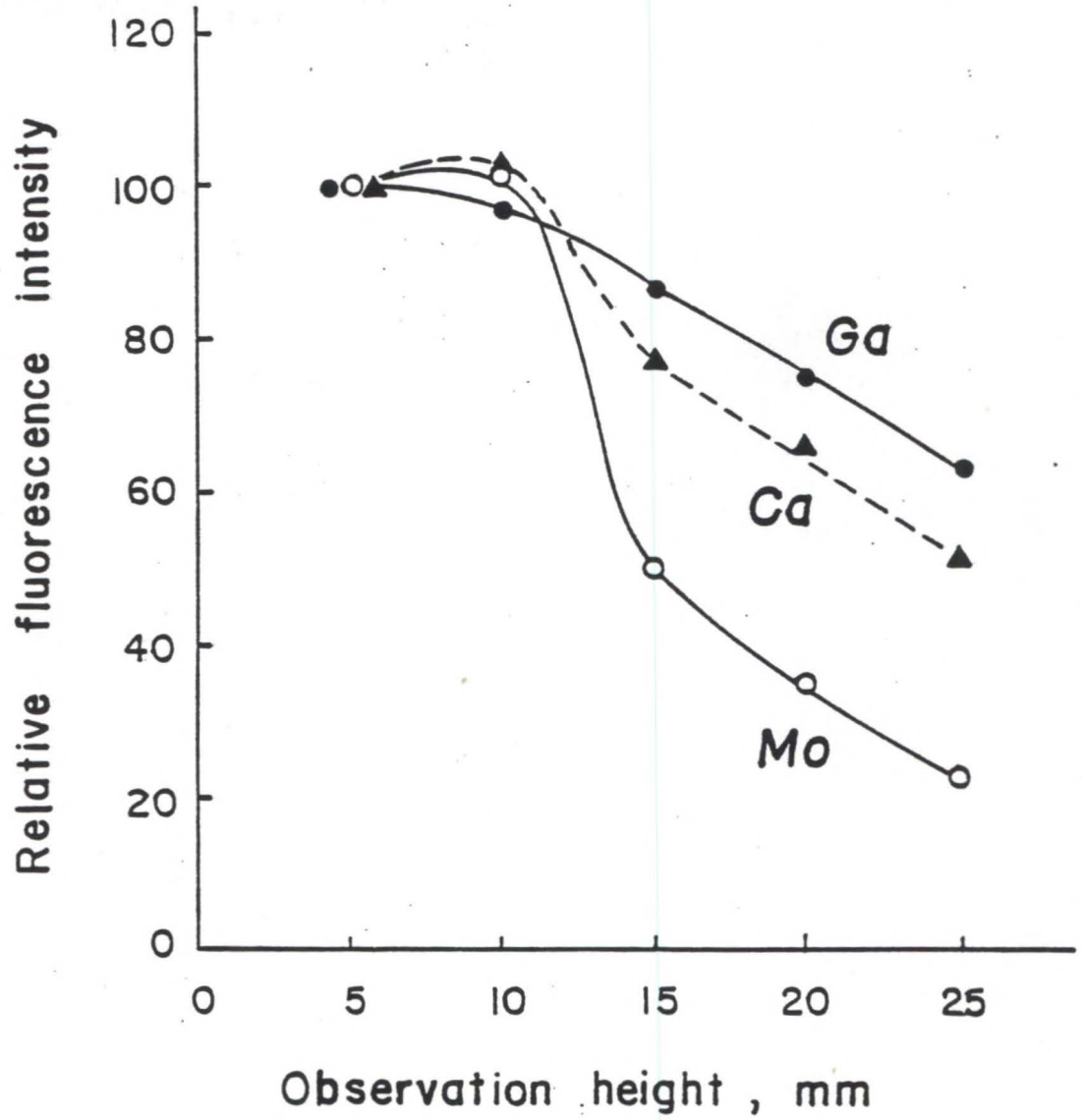

Figure 2-12. Vertical distributions of fluorescence intensities. Extended-sleeve torch used. Fluorescence lines: Ga(I) 403.3/403.3 nm (0.7 kW), Mo(I) 386.4/386.4 nm (1.0 kW), Ca(II) 393.4/393.4 nm (1.0 kW). (Observation height is position above the top of the extended-sleeve torch.)

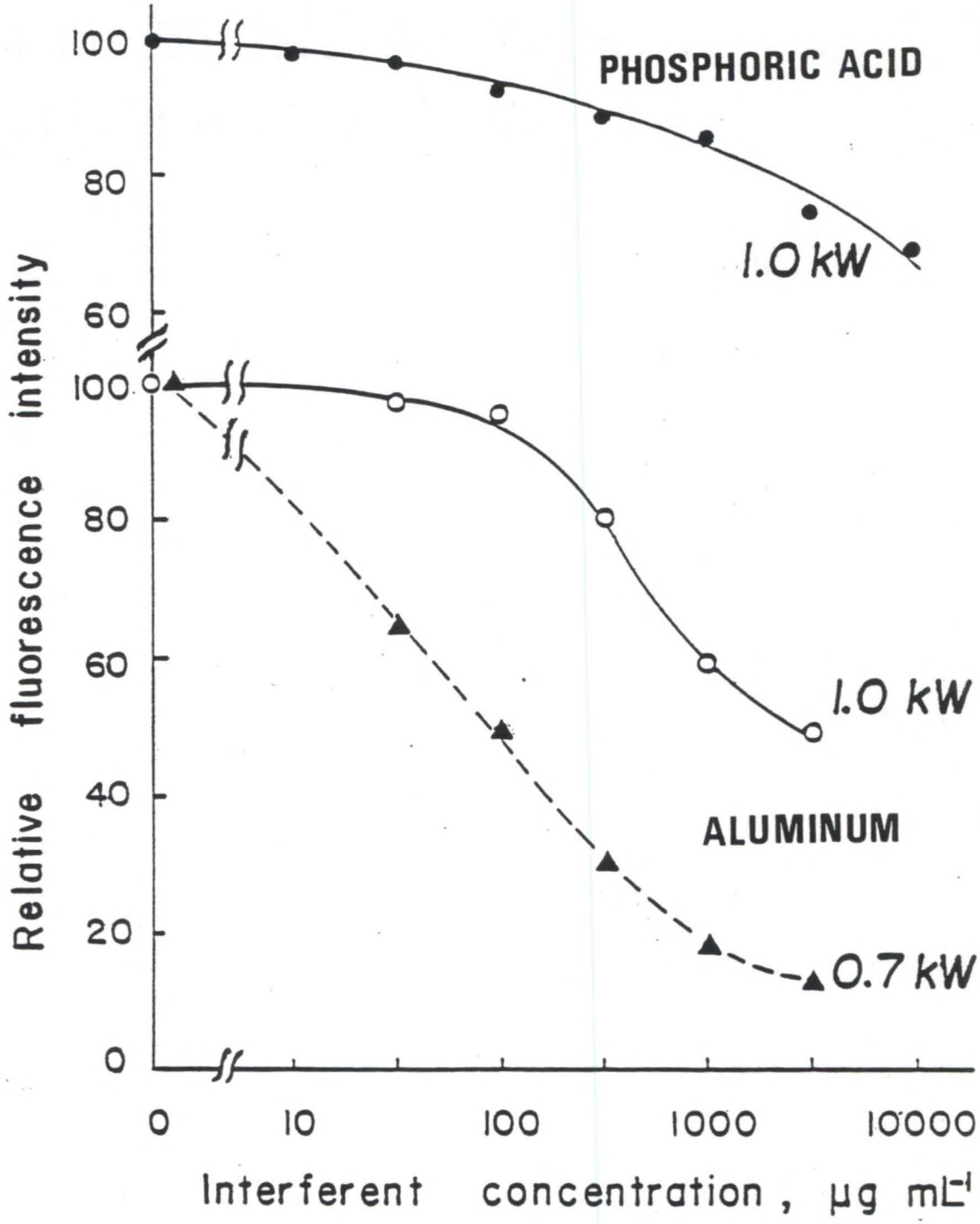

Figure 2-13. Effect of coexisting phosphorus and aluminum on resonance fluorescence intensities for calcium ion at 393.4 nm. Observation height: 5 mm above the top of the extended-sleeve torch (45 mm above the load coil).

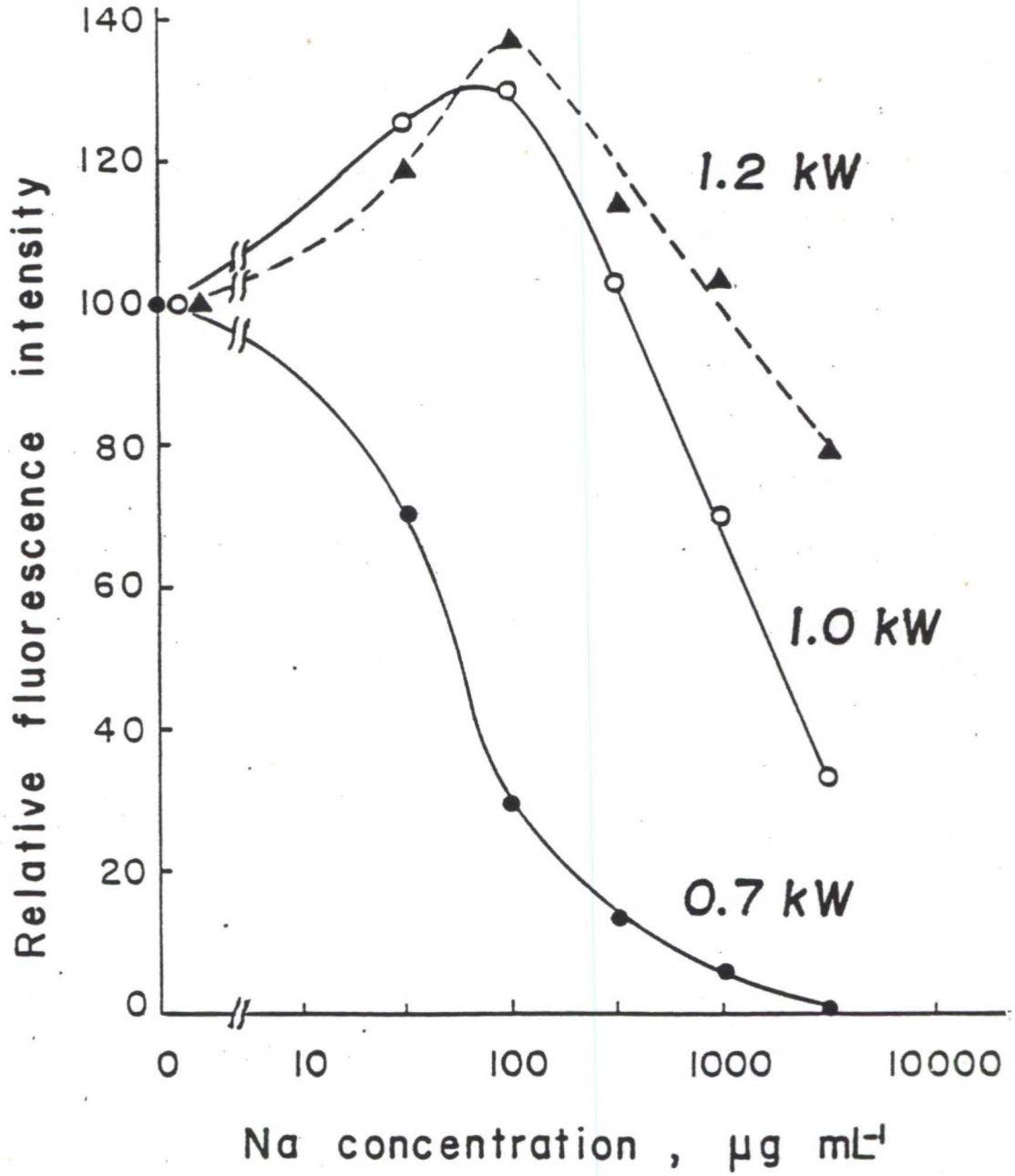

Figure 2-14. Effect of coexisting sodium on resonance fluorescence intensities for calcium ion at 393.4 nm. Observation height: 5 mm above the top of the extended-sleeve torch (45 mm above the load coil).

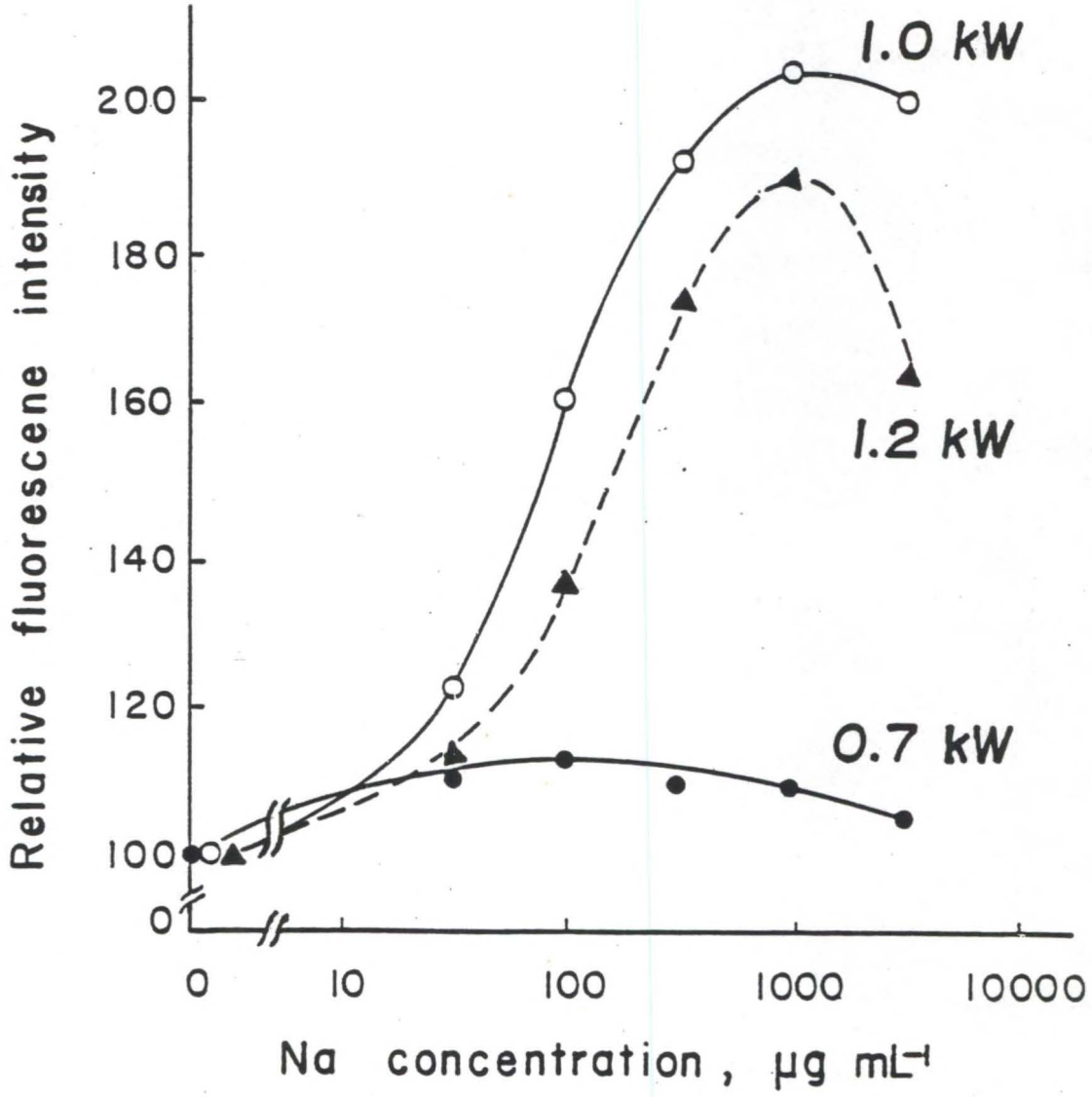

Figure 2-15. Effect of coexisting sodium on resonance fluorescence intensities for lead at 405.8 nm. Observation height: 5 mm above the top of the extended-sleeve torch (45 mm above the load coil).

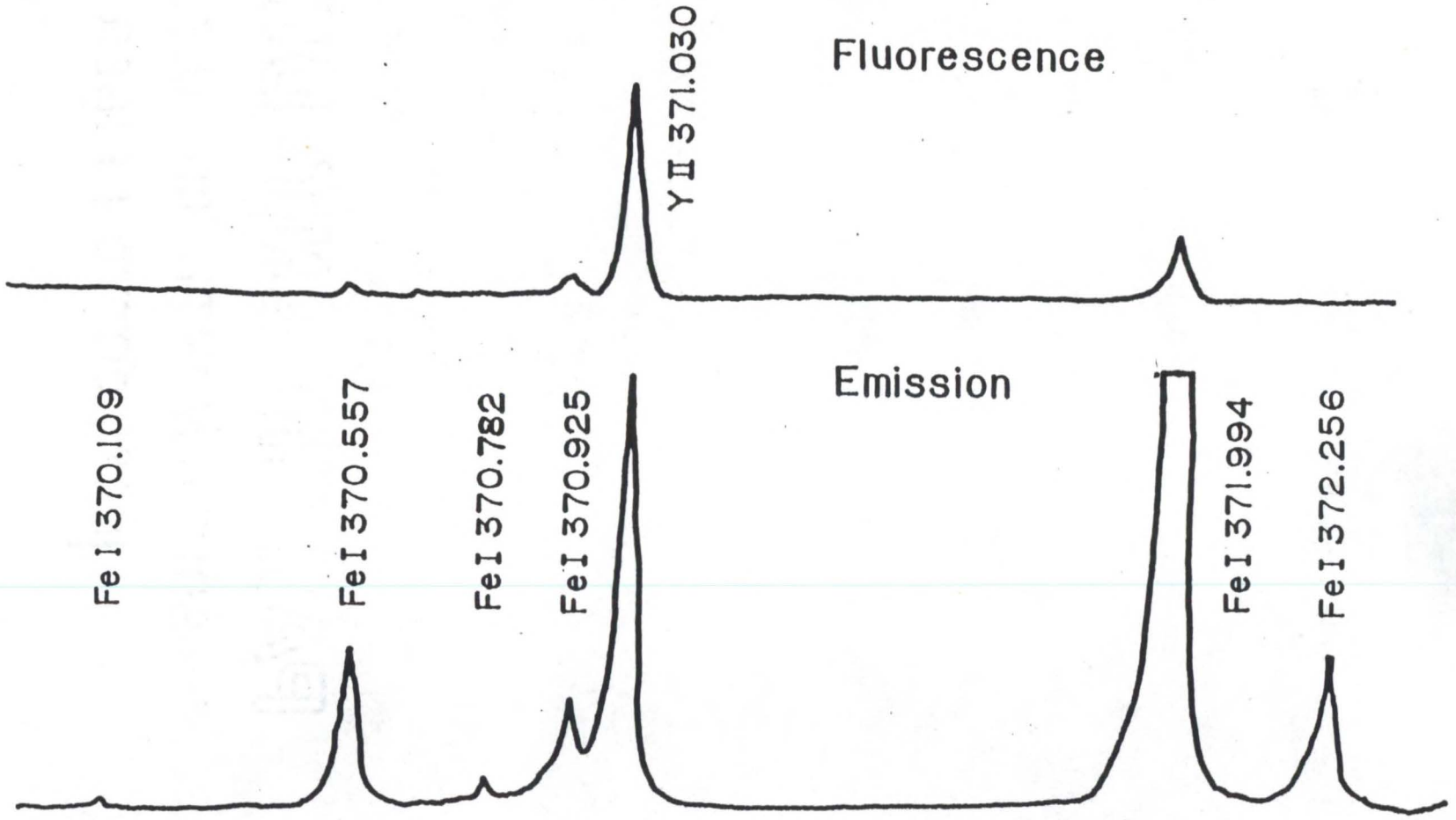

Figure 2-16. Emission and fluorescence excitation spectra for a 100 µg/mL yttrium solution in a 5000 µg/mL iron matrix. Conventional short torch used for emission and extended-sleeve torch for fluorescence. Spectral bandpass: 2 nm (fluorescence), 0.04 nm (emission).

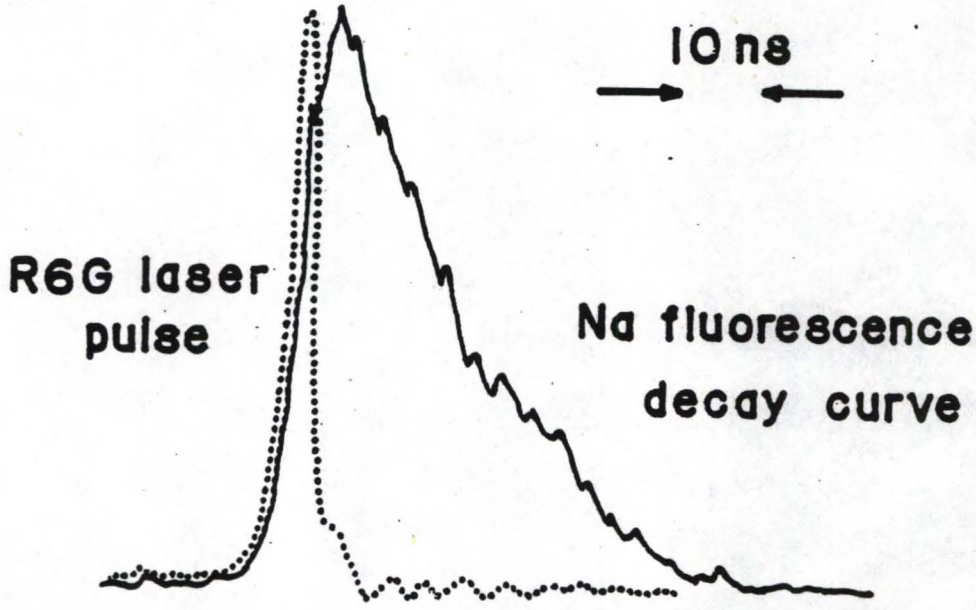

Figure 2-17. Decay time signals of the dye laser and sodium fluorescence at 589.0 nm. Observation height: 5 mm above the top of the extended-sleeve torch (45 mm above the load coil). Measured lifetime: 16 ns.

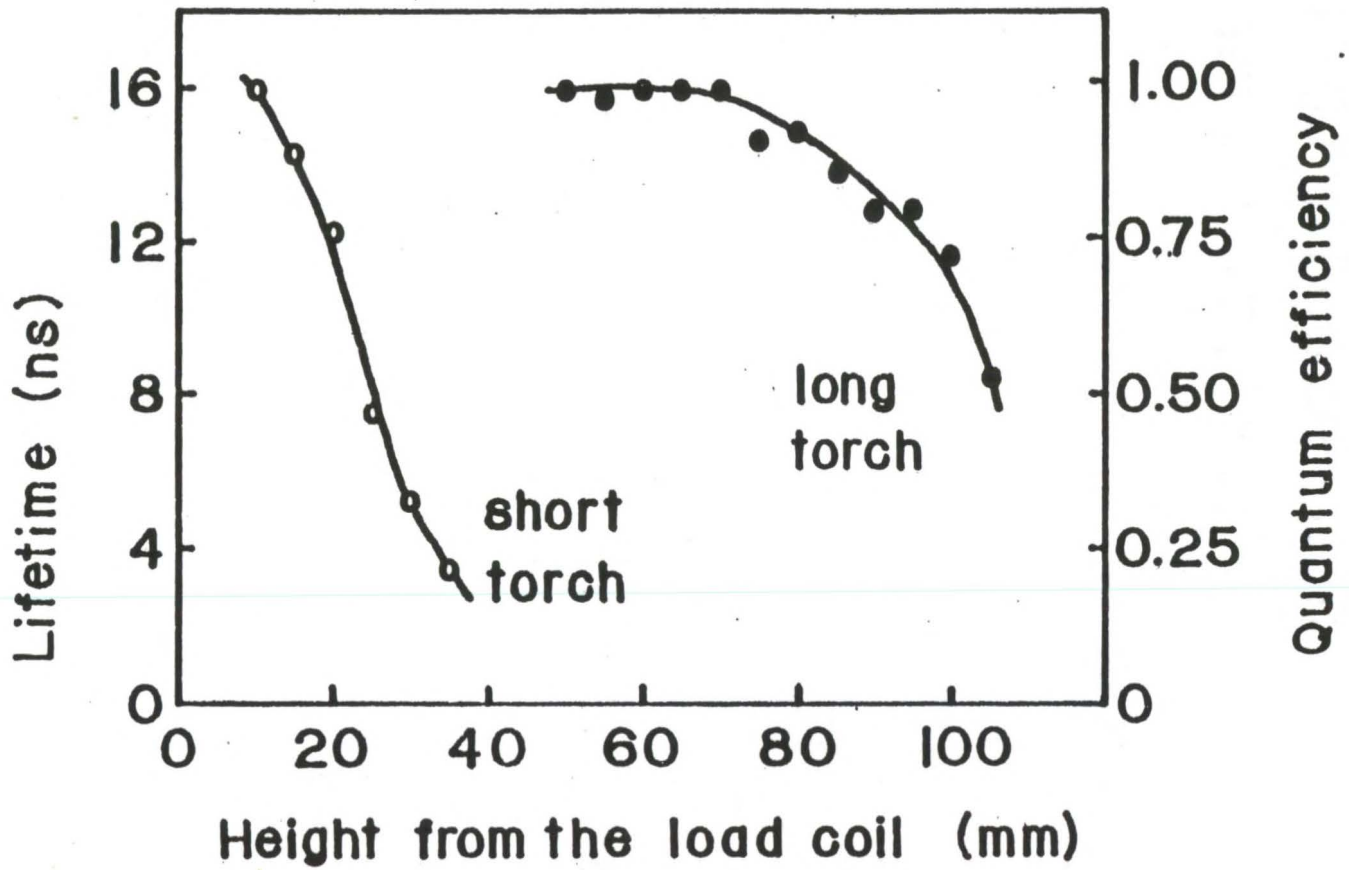

Figure 2-18. Vertical distributions of measured lifetimes and calculated quantum efficiencies for sodium using conventional (short) and extended-sleeve (long) torches.

CHAPTER III
ANALYTICAL STUDIES OF LASER-EXCITED ATOMIC AND IONIC FLUORESCENCE

Introduction

Laser-excited atomic fluorescence spectroscopic techniques were first established in a flame (27, 43, 47-51). Recently, a pulsed nitrogen-laser pumped tunable dye laser was used to excite atomic fluorescence in a flame resulting in an improvement of detection limits compared to conventional light sources (9). The available wavelength region of the dye laser is commonly 350 to 800 nm, although frequency doubling can be applied to achieve the range from ~220 to 350 nm. Some of the ICP's excellent characteristics as an emission source seem to be applicable as an atomization or ionization cell for fluorescence spectrometry. Further, spectral interferences, a major disadvantage in ICP emission spectrometry, might be reduced owing to the narrow spectral bandwidth of the laser output.

The first study using the ICP as an atomization cell for fluorescence was reported by Montaser and Fassel (52), where EDLs were used as excitation sources and special torches with extended-sleeves were investigated

for fluorescence measurements. Montaser and Fassel studied only cadmium, zinc and mercury for which intense EDLs were available. Demers and Allemand (53) and Demers et al. (54) investigated pulsed-HCLs for excitation of atomic fluorescence in the ICP and reported detection limits for 32 elements (with linear dynamic ranges of 4-5 orders of magnitude) that were comparable to flame-AAS.

Theoretical Considerations

In this work, a pulsed tunable dye laser-excited ICP system was employed. Such a system has the advantages of (i) high spectral irradiance; (ii) pulsed output; (iii) narrow spectral bandwidth of the excitation source; (iv) wide range of wavelength tunability; (v) high beam collimation; and (vi) minimization of ICP emission background noise. For resonance fluorescence, scattered radiation can result in a poor signal-to-noise ratio (SNR) and, consequently, a degradation of detection powers. However, for the case of non-resonance fluorescence, the detection powers will be limited by amplifier noise and/or dark current noise and/or ICP emission background noise and/or molecular fluorescence background noise. The narrow spectral bandwidth of the laser, and thus of the monochromator, as well as gated detection minimizes the ICP emission background noise. This allows the use of a measurement

system with a large optical throughout. For diagnostical measurments in the ICP such as spatial distributions of analyte species and temperature measurements in a small volume, a small diameter laser beam is essential. However, in the case of analytical studies, a highly collimated laser beam does not have a significant advantage over an expanded beam. The dependence of the fluorescence signal on the type and intensity of the excitation source has been treated extensively in the literature (55, 56). Beer's law is strictly valid only for zero incident light flux and, consequently, is accurate only for low intensity excitation sources. The use of a high intensity laser, however, results in the redistribution of the population of levels involved in the absorption process to the point where no more absorption occurs. At this point, the absorption coefficient decreases to zero as the process of stimulated emission balances that of absorption. This effect is commonly known as saturation of the optical transition (51, 57-60). In fact, using spectral irradiances higher than the saturation spectral irradiance for a given volume illuminated will only serve to double the fluorescence signal, at best. On the other hand, the source scatter signal will continue to increase linearly with source power. Therefore, if near saturation of the optical transition can be achieved with an expanded

laser beam, this would be beneficial since the fluorescence signals will increase in proportion to the volume of the plasma illuminated. The proportional dependence of the fluorescence signal upon n_2 (the number of excited-state atoms per unit volume) is given by (61)

$$B_F = n_2 h\nu_o (\ell/4\pi)(\tau_{sp})^{-1} \qquad (3\text{-}1)$$

where B_F = absolute fluorescence radiance (erg s^{-1} cm^{-2} sr^{-1});

h = Planck's constant (6.626×10^{-27} erg s);

ν_o = frequency of exciting radiation (s^{-1});

ℓ = depth of the homogeneous fluorescing volume in the direction of observation (cm); and

τ_{sp} = radiative lifetime (s).

For the sake of simplicity, the atomic system described here will be characterized as a collection of atoms having only two energy levels, 1 and 2, with equal statistical weights and without multiplet splitting. The levels are separated by the energy difference $\Delta E = h\nu_o \geq 2$ eV and have populations n_1 and n_2 (number of atoms per unit volume) with $n_1 + n_2 = n_T$ where n_T is the total density of atoms. Some assumptions made are (i) atoms are present as a trace component in a gas of molecules at a temperature of 2000-

5000K; (ii) the laser pulses have no effect on the energy distribution of the gas molecules, the velocity of the atoms, or the temperature of the system; (iii) coherence effects between absorbed and emitted photons are neglected; (iv) polarization effects are neglected; (v) homogeneity is achieved with regard to atomic concentration and temperature and (vi) the source radiation density is constant over the absorption line width (i.e., a spectral continuum). There are two analytically limiting cases with regard to the fluorescence signals obtainable.

Case 1: Low Spectral Irradiance

When the source spectral irradiance (E_{ν_o}) is much less than the saturation spectral irradiance ($E_{\nu_o}{}^{s}$) the fluorescence radiance expression becomes (61)

$$B_F = (\ell/4\pi)\, Y_{21}\, E_{\nu_o} \left[\int k(\nu) d\nu\right] \qquad (3\text{-}2)$$

where Y_{21} = quantum efficiency (dimensionless);

E_{ν_o} = source spectral irradiance (erg s^{-1} cm^{-2} Hz^{-1}); and

$k(\nu)$ = frequency-dependent absorption coefficient of the atomic vapor (cm^{-1}).

Equation 3-2 illustrates the linear dependence of the fluorescence signal on the source spectral irradiance and the quantum efficiency.

Case 2: High Spectral Irradiance

When $E_{\nu_o} >> E_{\nu_o}^{s}$, for steady-state conditions we have (61)

$$B_F = (\ell/4\pi)\ Y_{21}\ E_{\nu_o}\ \left[\int k^*(\nu)d\nu\right] \qquad (3\text{-}3)$$

where

$$k^*(\nu) = k(\nu)\left[E_{\nu_o}^{s}/E_{\nu_o} + E_{\nu_o}^{s}\right] \qquad (3\text{-}4)$$

In the case of laser excitation, E_{ν_o} can approach $E_{\nu_o}^{s}$ or even become larger. If $E_{\nu_o} >> E_{\nu_o}^{s}$, then equation 3-3 becomes

$$(B_F)_{MAX} = (\ell/4\pi)\ Y_{21}\ E_{\nu_o}^{s}\ n_T\ \left[\int\sigma(\nu)d\nu\right] \qquad (3\text{-}5)$$

where $(B_F)_{MAX}$ = maximum fluorescence radiance obtainable (erg s^{-1} cm^{-2} sr^{-1});

$E_{\nu_o}^{s}$ = saturation spectral irradiance (erg s^{-1} cm^{-2} Hz^{-1});

n_T = total atom number density (cm^{-3}); and

$\sigma(\nu)$ = frequency dependent absorption cross section (cm^2).

Therefore, when $E_{\nu_o} = E_{\nu_o}{}^s$, B_F becomes equal to $(B_F)_{MAX/2}$.

Analytical Curves of Growth

At low atomic concentrations (low optical densities), the integrated radiance of the fluorescence signal is linearly related to the atomic concentration. At high atomic concentrations (high optical densities), the analytical curve of growth (log of fluorescence intensity vs log of concentration) exhibits a zero slope in the case of continuum excitation and a negative slope in the case of line source excitation. The geometry of illumination and observation also plays a critical role in determining the shape of the analytical curve of growth. A prefilter effect may result because of a decrease in energy of the excitation beam in a region that is not observed by the detector. Also, a postfilter effect occurs if there is an unexposed region between the illuminated volume and the detector. For the present analytical studies, a focused laser beam (3 mm diameter) and an expanded laser beam (10 mm diameter) along with two different torch designs were examined to determine the optimal operating conditions for trace element analysis

using the laser-excited ICP-AFS system. The 10 mm beam was used to minimize postfilter effects and increase the fluorescence signals.

Experimental

Instrumentation

The instrumentation used in the analytical study is the same as that previously described in Chapter II for the diagnostical studies. The operating parameters for the two different torch designs follow.

Short torch. The RF power of the ICP was 1.0 kW and the plasma support argon flow rate was 15 L min^{-1}. Auxiliary argon was not used. The cross-flow nebulizer with a nebulizing gas pressure of 22 psig produced a carrier argon gas flow rate of approximately 1 L min^{-1}. The diameter of the dye laser beam at the plasma center was approximately 3 mm. The entrance and exit slit widths of the monochromator were 1 mm and the slit height was 3 mm. The observation region in the plasma was located 20 mm above the load coil.

The presence of minute water droplets at observation heights less than 15 mm above the load coil increases the background intensity in resonance fluorescence measurements (12). In flame atomic fluorescence spectrometry, a beam expander, light baffles and light traps

reduced the scatter signal level (9); no attempt to reduce scatter by those means was carried out here.

Extended-sleeve torch. The RF powers were 0.7 kW for the atomic lines of calcium, gallium, strontium, thallium and lead and 1.0 kW for the atomic lines of aluminum, molybdenum, vanadium and for all the ionic lines, except for the lines of yttrium and zirconium where 1.2 kW was used. The plasma support argon flow rate was 15 L min^{-1} and auxiliary argon was not used. The cross flow nebulizer was operated at 40 psig and produced a carrier argon gas flow rate of approximately 1.7 L min^{-1}. The diameter of the dye laser beam at the plasma center was approximately 10 mm. The entrance and exit slit widths of the monochromator were 1 mm and the slit height was 10 mm. The center of the expanded dye laser beam was located 10 mm from the top of the torch in order to avoid hitting the torch and increasing the scatter signal.

Chemicals

Stock solutions of 1000 μg mL^{-1} were prepared from the pure metal when possible or from reagent grade chemicals, dissolved in the minimum amount of acid and successively diluted with distilled/deionized water.

Results and Discussion

Fluorescence intensities in the ICP depend primarily on the following three factors: (i) number density of the lower level in the laser excitation process; (ii) output power (spectral irradiance) of the laser and (iii) the spontaneous transition probability of the fluorescence line. Laser excitation from the ground-state and saturation of the optical transition are both advantageous. In this study, sensitive lines below 350 nm were not considered because of poor laser energy in the frequency doubled mode and difficulty encountered in keeping the doubled line tuned.

Analytical Application of the ICP Using a Conventional Short Torch as an Atomization and Ionization Cell for Fluorescence Spectrometry

The ICP as an atomization and ionization cell, because of the high temperature and high electron number density, is effective for reducing the chemical and ionization interferences observed in flame-AFS. Also, AFS is effective for avoiding spectral interferences observed in ICP emission spectrometry.

The detection limits for ICP-AFS and ICP-AES obtained with all operating parameters the same, except for the slit widths of the monochromator (0.1 mm for emission), are compared in Table 3-1. The limits of

detection are the concentrations corresponding to a signal twice the standard deviation of the background obtained from sixteen consecutive 10s integrated blank (water) readings. The detection limits for fluorescence are about two orders of magnitude higher than those in emission. However, fluorescence detection limits seem to be sufficient for trace analysis without spectral interference. The fluorescence analytical curves of growth have a linear dynamic range of 3-4 orders of magnitude.

Generally, the temperature of the analytical emission region (10-25 mm above the load coil) in the ICP is too high for fluorescence measurements. The high temperature results in high populations of excited levels which are sometimes effective for excited-state fluorescence; however, the strong emission background and noise can cause problems. One method to decrease the temperature is to increase the carrier argon flow rate while using an observation height of 10-25 mm above the load coil. However, at high carrier argon flow rates (>1.5 L min^{-1}), the plasma might not be in LTE at lower heights due to insufficient collisional energy transfer between plasma and analyte species (41). Consequently, insufficient gas kinetic energy leads to interelement effects in the presence of the alkali elements (33).

Measurements at higher positions(50-80 mm above the load coil) are also useful because LTE should be more nearly established and chemical and ionization interferences should be negligible. This technique has already been applied using HCLs as light sources (53) and an extended-sleeve torch in order to minimize analyte atom diffusion and to maintain good signal stability. Analytical studies using an extended-sleeve torch will be discussed next.

Analytical Application of the ICP Using an Extended-Sleeve Torch as an Atomization and Ionization Cell for Fluorescence Spectrometry

The fluorescence intensity for Ca(II) at 393.4 nm using a 40 psig nebulizing gas pressure was about four times larger than that obtained at the 30 psig nebulizing gas pressure. This result was similar for other atomic and ionic lines. At high observation points above the load coil, the analyte number density becomes less than in lower positions due to diffusion, as is shown in emission (10), absorption (41) and fluorescence measurements (12). An extended-sleeve torch was used in order to minimize diffusion of the analyte atoms into the surrounding air. Furthermore, this torch should be more effective than the short torch for collisional energy transfer from the plasma to the analyte atoms (41).

For the improvement of the fluorescence sensitivity, the use of an expanded dye laser beam (about 10 mm diameter) and a 10 mm monochromator slit height were investigated. Fluorescence intensities were 3-5 times larger than those in the case of the 3 mm diameter laser beam and 3 mm monochromator slit height using the same extended-sleeve torch. Background intensity caused by scattering also increased; however, the increase in the noise level was small. As a result, the fluorescence SNR was improved by several times. The SNR was markedly improved at non-resonance lines.

In Table 3-2, limits of detection for laser-excited ICP-AFS together with those obtained by ICP-AES by Boumans and Bosveld (62) are given. With the present method, ionic fluorescence is generally more sensitive than atomic fluorescence for the same element as is shown for barium, calcium and strontium. In the case of vanadium, the ionic line is less sensitive, probably because laser excitation occurs from an excited-state which is not well-populated. This might also be true of zirconium, although no data on atomic fluorescence for this element was obtained.

Comparing LODs using an extended-sleeve torch with those obtained under the conditions of 1.0 kW RF power, 22 psig nebulizing gas pressure and 20 mm observation height using the conventional short torch,

we can see from Table 3-3 that the short torch provided superior LODs for ionic excited-state fluorescence as is shown for yttrium and vanadium. For the other lines, LODs are improved by 1-3 orders of magnitude for fluorescence with the extended-sleeve torch over the short torch. Calibration curves were obtained using the extended-sleeve torch and indicated 4 orders of magnitude of linearity from the LOD levels. The linearity was extended to higher concentrations by 1-2 orders of magnitude by decreasing the light introduced to the monochromator through the use of neutral density filters.

Conclusions

The short torch is best utilized in laser-excited ICP-AFS for excited-state fluorescence owing to its higher temperature as compared to an extended-sleeve torch. However, strong emission background is observed with the short torch and can cause problems such as detector saturation. Consequently, an extended-sleeve torch is more useful in laser-excited ICP-AFS for the analytical study of atomic and ionic fluorescence other than excited-state fluorescence. This torch also minimizes diffusion of the analyte atomic vapor into the surrounding air.

For analytical studies, an expanded dye laser beam is beneficial in the respect that the fluorescence

signal will be proportional to the volume of the plasma illuminated. A 10 mm diameter laser beam was found to be optimal in this work.

Table 3-1. Detection Limits for ICP-AFS and ICP-AES

Species	Laser-ICP-AFS[1] Ex λ/Fl λ[3] (nm)	LOD[4] (ng mL^{-1})	ICP-AES[2] Em λ (nm)	LOD (ng mL^{-1})
Ba(II)	455.403	40	455.403	0.7
Ca(II)	393.366	8	393.367	0.4
V(II)	390.326/290.882	700	290.882	30
Y(II)	508.742/371.030	30	371.030	1
Mo(I)	386.411	3000	386.411	10
Pb(I)	405.783	6000	405.783	70
Tl(I)	377.576	8000	377.572	60

[1]Short torch used; 3 mm diameter laser beam; 20 mm observation height above load coil; 1 mm monochromator slit width; 3 mm monochromator slit height.

[2]Short torch used; 20 mm observation height above load coil; 0.1 mm monochromator slit width; 3 mm monochromator slit height.

[3]Excitation wavelength/fluorescence wavelength (if different than excitation wavelength).

[4]Limit of detection.

Table 3-2. Detection Limits for ICP-AFS and ICP-AES.

Species	Laser-ICP-AFS[1] Ex λ/Fl λ[3] (nm)	LOD[4] ($ng\ mL^{-1}$)	ICP-AES[2] Em λ (nm)	LOD ($ng\ mL^{-1}$)
Al(I)	394.401/396.152	5	396.152	1
Ba(I)	553.548	2000		
Ba(II)	455.403	1	455.403	0.05
Ca(I)	422.673	100	422.673	3
Ca(II)	393.366	1	393.366	0.04
Ga(I)	403.298	10	403.298	5
	403.298/417.206	4	417.206	3
Mo(I)	386.411	100	386.411	2
Pb(I)	405.783	70	405.783	20
	405.783/283.306	100	283.306	40
Sc(II)	364.279	30	364.279	0.13
Sr(I)	460.733	6	460.733	2
Sr(II)	407.771	0.5	421.552	0.03
Tl(I)	377.576	8	377.576	11
	377.576/535.046	10	535.046	9

(continued)

Table 3-2. (continued)

Species	Laser-ICP-AFS[1] Ex λ/Fl λ[3] (nm)	LOD[4] ($ng\ mL^{-1}$)	ICP-AES[2] Em λ (nm)	LOD ($ng\ mL^{-1}$)
V(I)	411.178	400	411.178	9
V(II)	390.326/290.882	10,000	290.882	0.7
Y(II)	371.030	10	371.030	0.08
Y(II)	508.742/371.030	70		
Zr(II)	431.731/349.621	6000	349.621	0.9

[1]Extended-sleeve torch used; 10 mm diameter laser beam; 10 mm observation height above top of torch; 1 mm monochromator slit width; 10 mm monochromator slit height.

[2]Reported by Boumans and Bosveld (62).

[3]Excitation wavelength/fluorescence wavelength (if different from excitation wavelength).

[4]Limit of detection.

Table 3-3. Comparison of Detection Limits for Laser-Excited ICP-AFS Using Extended-Sleeve and Short Torches

Species	Laser-ICP-AFS[1] Ex λ/Fl λ[3] (nm)	LOD[4] ($ng\ mL^{-1}$)	Laser-ICP-AFS[2] Ex λ/Fl λ (nm)	LOD ($ng\ mL^{-1}$)
Al(I)	394.401/396.152	5		
Ba(I)	553.548	2000		
Ba(II)	455.403	1	455.403	40
Ca(I)	422.673	100		
Ca(II)	393.366	1	393.366	8
Ga(I)	403.298	10		
	403.298/417.206	4		
Mo(I)	386.411	100	386.411	3000
Pb(I)	405.783	70	405.783	6000
	405.783/283.306	100		
Sc(II)	364.279	30		
Sr(I)	460.733	6		
Sr(II)	407.771	0.5		
Tl(I)	377.576	8	377.576	8000
	377.576/535.046	10		

(continued)

Table 3-3. (continued)

Species	Laser-ICP-AFS[1] Ex λ/Fl λ[3] (nm)	LOD[4] ($ng\ mL^{-1}$)	Laser-ICP-AFS[2] Ex λ/Fl λ (nm)	LOD ($ng\ mL^{-1}$)
V(I)	411.178	400		
V(II)	390.326/290.882	10,000	390.326/290.882	700
Y(II)	371.030	10		
Y(II)	508.742/371.030	70	508.742/371.030	30
Zr(II)	431.731/349.621	6000		

[1]Extended-sleeve torch used.

[2]Short torch used.

[3]Excitation wavelength/fluorescence wavelength (if different from excitation wavelength).

[4]Limit of detection.

CHAPTER IV
ATOMIC AND IONIC FLUORESCENCE IN THE INDUCTIVELY COUPLED PLASMA (ICP) USING A SECOND ICP AS AN EXCITATION SOURCE

Introduction

The ICP has long been used as an effective vaporization, atomization, excitation and ionization (VAEI) cell for emission spectrometry (1). Many physical parameters of the ICP have been investigated and a review by Barnes (63) contains many references covering various operating principles of the ICP. However, due to complex emission spectra, a high resolution monochromator is needed in many cases to isolate the analytical lines of interest.

The first use of the ICP as an excitation source for flame-AFS was reported by Hussein and Nickless (64). Relatively poor detection limits were obtained, though. Since then, improvements in sample introduction and plasma stability have resulted in the further use of the ICP as an excitation source for flame-AFS. Epstein et al. (7) have shown that the advantage of the ICP compared to other AFS sources is its flexibility with respect to the intense atomic and ionic line radiation available. Changing from one element to the next is

simply done by aspirating a different solution into the source ICP.

Omenetto et al. (65) have examined the ICP emission profile by using the resonance monochromator method, in which a low concentration of analyte is aspirated into a flame and increasing concentrations are aspirated into the ICP. The resulting fluorescence from the flame is monitored and certain limiting characteristics of the ICP emission profile can be inferred.

The high intensity, long-term stability, narrow line width and freedom from self-reversal all contribute to the ICP being an excellent excitation source for AFS. Also, due to the narrow line width of spectral lines in the ICP, spectral interferences are not observed in AFS.

In this work, the utilization of the ICP as a source to excite atomic and ionic fluorescence in a second ICP was investigated (ICP-ICP-AFS). Excitation, emission and fluorescence analytical curves of growth were obtained and from these, further information about the line profile of the ICP was revealed. For the excitation curve of growth, a fixed, low concentration of the analyte was aspirated into the atomization ICP while increasing concentrations were introduced to the source ICP. For the conventional emission curve of growth, the emission from the source ICP was plotted

versus concentration and, thirdly, the fluorescence analytical curve of growth was obtained by aspirating a fixed high concentration (20 mg mL^{-1}) of the analyte into the source ICP while increasing concentrations were introduced to the atomization ICP. Vertical distributions of atomic and ionic species densities were obtained and detection limits for 16 elements are compared to the ICP-excited flame technique.

Further, a few examples of chemical and spectral interferences were examined. Finally, the noise sources limiting the measurements were investigated and suggested improvements are discussed.

Theoretical Considerations

The following "excitation function" (65) describes the interaction between the radiation emitted by the source ICP and the absorbing atoms in the atomization ICP:

$$\int_{abs} E_{\lambda_{exc}}(\lambda)\alpha_f(\lambda)d\lambda = \int_{abs} E_{\lambda_{exc}}(\lambda)\{1 - \exp\left[-k_f(\lambda)L\right]\}d\lambda \qquad (4\text{-}1)$$

The integral is extended over the entire absorption line width (i.e. the width over which $k_f(\lambda)$ differs markedly from zero).

where $E_{\lambda_{exc}}(\lambda)$ = spectral irradiance of the source ICP as a function of wavelength at a given height and analyte concentration, evaluated at wavelength λ ($J\ s^{-1}\ cm^{-2}\ nm^{-1}$);

$\alpha_f(\lambda)$ = fraction of radiation absorbed at any wavelength λ (dimensionless);

$k_f(\lambda)$ = absorption coefficient of analyte atoms in atomization ICP (cm^{-1}); and

L = interaction length for the absorption process in the atomization ICP (cm).

The spectral irradiance of the source ICP, $E_{\lambda_{exc}}(\lambda)$, can be taken as the product of the blackbody spectral irradiance at wavelength λ, and at the source ICP emission temperature, and the total absorption factor which is a function of the concentration in the source ICP and of its emission depth in the direction of the atomization ICP.

By observing the fluorescence in the atomization ICP, the fluorescence radiance is described by

$$B_F \propto \left\{ \int_{abs} E_{\lambda_{exc}}(\lambda)\{1 - \exp[-k_f(\lambda)L]\}d\lambda \right\} \left\{ \frac{\int_{abs}\{1 - \exp[-k_f(\lambda)\ell]\}d\lambda}{\ell \int_{abs} k_f(\lambda)d\lambda} \right\} \propto \left\{ \int_{abs} E_{\lambda_{exc}}(\lambda)\{1 - \exp[-k_f(\lambda)L]\,d\lambda \right\} \left\{ \frac{A_t(n_f\ell)}{\ell \int_{abs} k_f(\lambda)d\lambda} \right\} \right\} \qquad (4\text{-}2)$$

Equation 4-2 is equal to equation 4-1 multipled by a factor that takes into account self-absorption of fluorescence occurring in the atomization ICP. Here, $A_t\ (n_f \ell) \equiv \int\{1 - \exp[-k_f(\lambda)\ell]\}d\lambda$ is the total absorption factor for the fluorescence in the atomization ICP where n_f is the atomization ICP atomic concentration and ℓ is the (homogeneous) fluorescence depth. Equation 4-2 can be simplified for the limiting cases of line and continuum excitation sources.

Case 1: The ICP Acts as a Line Source

In this case, $k_f(\lambda)$ can be considered constant and equal to its peak value, k_{max_f}. If n_f is low, then equation 4-2 reduces to equation 4-3:

$$B_F \propto\{1 - \exp[-k_{max_f} L]\}\int E_{\lambda_{exc}}(\lambda)d\lambda \qquad (4\text{-}3)$$

The source ICP can act as a line source if its spectral emission profile is narrower than the absorption profile in the atomization ICP, even though its higher temperature would seem to cause Doppler broadening (see Chapter II regarding the temperature of the ICP using a short torch versus an extended-sleeve torch).

Case 2: The ICP Acts as a Continuum Source

In this case, at high atomic concentrations in the source ICP, self-absorption can broaden the emission profile to such an extent that it becomes larger than the absorption profile in the atomization ICP. In this case, if n_f is low, equation 4-2 reduces to equation 4-4:

$$B_F \propto E_{\lambda_{exc}} (\lambda_o) \int_{abs} \{1 - \exp [-k_f (\lambda) L]\} d\lambda \propto$$

$$E_{\lambda_{exc}} (\lambda_o) A_t (n_f L) \qquad (4\text{-}4)$$

where $E_{\lambda_{exc}} (\lambda_o)$ is the constant irradiance of the source ICP over the absorption line profile.

Discussion of Both Cases

For the source ICP emission curve of growth, a limiting slope of unity at low atom densities and a slope of 0.5 at high atom densities can be expected in the absence of self-reversal.

For the excitation curve of growth in the absence of self-reversal, if a constant low concentration of analyte is aspirated into the atomization ICP and the fluorescence radiance monitored while aspirating increasing concentrations into the source ICP, a limiting slope of unity for low atom densities and a slope of zero at high atom densities in the source ICP can be predicted. If

self-reversal does occur, a negative slope will be observed in the experimental plot.

For the case of the fluorescence curve of growth, if the source ICP acts as a line source, a limiting slope of unity will be observed for low atom densities in the atomization ICP and a slope of -0.5 for high atom densities. This would indicate that the source ICP spectral emission profile is narrower than the absorption profile in the atomization ICP.

If the source ICP acts as a continuum source, then a limiting slope of unity at low atom densities in the atomization ICP and a slope of zero at high atom densities should be observed. The absence of self-reversal can be inferred by the combined observation of the fluorescence curve of growth and the excitation curve of growth obtained under the same experimental settings.

These results have been previously summarized (65) and can be obtained from equations 4-2, 4-3 and 4-4 by assuming that the self-absorption factor for the fluorescence cannot be considered negligible and remembering that A_t (n_f L) and A_t(n_f ℓ) vary linearly with n_f at low n_f values and with $n_f^{\frac{1}{2}}$ at high n_f values.

Experimental

Instrumentation

A block diagram of the experimental system is given in Figure 4-1.

The source ICP(Plasma-Therm 2500D, Kresson, NJ) utilized a conventional short torch (Plasma-Therm T 1.0) and was operated at 2.0 kW RF power, 15 L min^{-1} plasma support argon flow rate, 1.5 L min^{-1} auxiliary argon flow rate and 20 psig nebulizing gas pressure. A 20 mg mL^{-1} analyte excitation solution was used. Two exceptions, however, were aluminum and sodium. Aspiration of 20 mg mL^{-1} solutions of aluminum and sodium clogged the pneumatic nebulizer (Plasma-Therm PN 5601) after only a few minutes of operation. For these elements, a 10 mg mL^{-1} excitation solution was used to avoid clogging.

The atomization ICP (Plasma-Therm 1500D) utilized an extended-sleeve torch (Baird Corp., Bedford, MA) and was operated at 0.7 kW for the atomic lines and 1.0 kW for the ionic lines of non-refractory elements, as well as the atomic and ionic lines of refractory and rare earth species. The exception in this case is vanadium for which 1.2 kW was used. The plasma support argon flow rate was 15 L min^{-1}, no auxiliary flow was used and the penumatic nebulizer gas pressure was 35 psig (J.E. Meinhard Assoc. T-230-A3, Santa Ana, CA). The observation height in the atomization ICP for the atomic lines of non-refractory elements was 40 mm above the top of the extended-sleeve torch (80 mm above the load coil since the outer sleeve of the torch extends for 40 mm beyond the top of the load coil). The observation height for all other lines

was 20 mm above the top of the torch (60 mm above the load coil).

The radiation obtained (between 10-30 mm above the load coil) by aspirating 20 mg mL^{-1} aqueous solutions of the analyte into the source ICP was chopped at a frequency of 550 Hz (Rofin-Math Assoc. 7500, Great Neck, NY) and focused onto the atomization ICP through the use of spherical quartz S1-UV grade lenses (50 mm diameter, 75 mm focal length). The resultant fluorescence was observed at a 90 degree angle with a 350 mm focal length monochromator (Heath Co. EU-700; now GCA Corp., McPherson Instruments, Acton, MA). The entrance and exit slit widths were 1 mm and the slit height was 10 mm. The photomultiplier tube (Hamamatsu, Inc. R928, Middlesex, NJ) was operated at -1000V (Pacific Precision Instruments HV Supply, Concord, CA), the output of which was pre-amplified (Keithley Instruments, Inc. 427, Cleveland, OH) and fed to a lock-in amplifier (Ithaco, Inc. Dynatrac 391, Ithaca, NY) and then to a laboratory-constructed integrator. The 10s integrations were displayed on a digital voltmeter (John Fluke Mfg. Co., Inc. 8000A, Seattle, WA). For the spectral interference study, the output of the lock-in was fed to a chart recorder (Fisher Scientific Co. 5000, Pittsburgh, PA). Neutral density filters allowed verification of the linearity of the fluorescence and emission photomultiplier response.

Chemicals

Stock solutions of 20 mg mL^{-1} were prepared from the pure metal when possible or from reagent grade chemicals, dissolved in the minimum amount of acid and successively diluted with distilled/deionized water.

Results and Discussion

Vertical Distributions of Atomic and Ionic Fluorescence Intensities

In Figure 4-2, vertical distributions are given for zinc atomic and calcium ionic fluorescence intensities. The fluorescence intensity at 5 mm above the top of the extended-sleeve torch was taken to be the same for both elements. However, the signal-to-noise ratio was found to be poor at this height. Consequently, an observation height of 40 mm above the top of the extended-sleeve torch (80 mm above the load coil) was adopted for zinc and was also found to be optimal for the other atomic lines of non-refractory elements. It can be seen from Figure 4-2 that beyond 80 mm above the load coil, the zinc fluorescence intensity drops off rapidly due to quenching by air entrainment in the plasma (see Chapter II).

For all other lines, a 20 mm observation height above the top of the extended-sleeve torch (60 mm above the load coil) was found to be optimal.

Above this height, the fluorescence intensity for these lines becomes very weak due to the decrease in temperature of the plasma and air entrainment (see Chapter II).

Analytical Curves of Growth

In Figures 4-3 and 4-4, the excitation and emission curves of growth for zinc and calcium are shown. As has been previously shown for both elements in ICP-excited flame-AFS (65), the excitation curves of growth yield a limiting slope of unity at low atom densities in the source ICP and a slope approaching zero at high atom densities. Also, the emission curves of growth for both elements yield a limiting slope of unity at low atom densities in the source ICP and a slope of 0.5 at high atom densities. The limiting slopes of Figures 4-3 and 4-4 agree well with theory (65) and show that self-reversal is absent in the ICP under the conditions used in this study. In Figure 4-5, fluorescence analytical curves of growth are given for zinc and calcium; these curves show that at low atom densities in the atomization ICP, a limiting slope of unity is obtained while at high atom densities a slope of -0.5 is obtained. According to theory (65), the source ICP is acting as a "line" excitation source compared to the absorption profile in the atomization ICP, even though the higher temperature of the source ICP (2.0 kW RF

power, short torch) would seem to cause the Doppler half-width to be larger than that of the cooler atomization ICP (< 1.2 kW RF power, extended-sleeve torch). It has been previously shown (see Chapter II) that the temperature of the plasma using an extended-sleeve torch is about 1000-1500K less than the plasma using a short torch, depending on the RF power and observation height.

The temperatures of the plasma were obtained at the two heights and three RF powers used in this study from a three-line slope calculation using iron atomic emission lines at 382.0, 382.4 and 382.6 nm. Spectral data with respect to these lines have been summarized previously (33). The temperatures were found to be: (i) 3290K (0.7 kW, 40 mm observation height above top of extended-sleeve torch); (ii) 3540 K (1.0 kW, 20 mm observation height); and (iii) 3810 K (1.2 kW, 20 mm observation height).

Limits of Detection

As shown in Table 4-1, limits of detection for many of the elements investigated are within one order of magnitude for the best reported detection limits using the ICP as an excitation source for flame-AFS (7).

Interelement Effects

In Figure 4-6, some chemical interferences observed on calcium ionic fluorescence at 393.4 nm are shown (atomization ICP 1.0 kW, 20 mm observation height above top of extended-sleeve torch). It can be seen from Figure 4-6 that there is an enhancement in calcium ionic fluorescence intensity with the addition of aluminum and sodium, possibly due to a change in the atom and ion distributions in the plasma (42). Similar enhancements with the addition of sodium were observed at high carrier argon flow rates (>1.0 L min^{-1}) at 15 mm above the load coil with a conventional short torch in the ICP (33). The signal suppression at high aluminum concentrations is primarily due to the increase in sample solution viscosity (2, 3).

In combustion flames, the presence of phosphorus sometimes results in the formation of refractory compounds, causing a consequent decrease in the fluorescence signal. In Figure 4-6, the effect of the presence of phosphorus on calcium ionic fluorescence intensity is shown. The intensity was slightly suppressed by the presence of phosphorus, being due mostly to the increase in sample solution viscosity (2, 3).

Spectral Interferences

One of the advantages in ICP-ICP-AFS should be relative freedom from spectral interferences due to the

narrow spectral bandwidth of spectral lines in the ICP. Three cases of spectral overlap were investigated: (i) Zn (213.856 nm) and Cu (213.853 nm); (ii) Yb (369.419 nm) and Sm (369.399, 369.430 nm); and (iii) Co (231.160 nm) and Ni (231.096, 231.234 nm). The results obtained are summarized in Table 4-2.

Difficulty is encountered in the measurement of zinc in a copper matrix by atomic absorption or ICP-AES since the zinc resonance line at 213.856 nm is subject to direct interference from the copper non-resonance line at 213.853 nm. This interference has been reported (66) for flame atomic absorption analysis and requires elaborate procedures to remove the copper prior to analysis. Even with an echelle spectrometer (spectral bandpass = 0.003 nm), this line pair has been shown to exhibit an overlap (67).

The measurement of a 10 $\mu g\ mL^{-1}$ Zn solution in a 5000 $\mu g\ mL^{-1}$ Cu matrix using a 20 $mg\ mL^{-1}$ Zn solution for excitation resulted in no significant excitation of copper fluorescence using a monochromator spectral bandpass of 2 nm. In addition to the line radiation emitted by the source ICP, the copper non-resonance transition at 213.853 (11203-57949 cm^{-1}) is difficult to excite due to the high excited lower level of this transition.

Ytterbium and samarium are also subject to spectral interference problems. As shown in Figure 4-7, emission spectral lines at Yb(II) 369.419 nm and Sm(II) 369.399 nm overlap. In this case, a 100 μg mL^{-1} Yb solution containing a 1000 μg mL^{-1} Sm matrix was excited by the radiation emitted by a 20 mg mL^{-1} Yb solution in the source ICP. No observable difference in fluorescence intensity was seen between this solution and a 100 μg mL^{-1} Yb solution while using a monochromator spectral bandpass of 2 nm. The only observable difference was the increase in the background noise level due to the Sm matrix solution.

Lastly, nickel and cobalt are subject to spectral interference problems in the wavelength region of 231 nm. The radiation emitted from the source ICP while aspirating a 20 mg mL^{-1} solution of cobalt was used to excite a solution containing 1000 μg mL^{-1} Co and 1000 μg mL^{-1} Ni. On the other hand, the radiation emited from a 20 mg mL^{-1} Ni solution was also used to excite this same solution. As can be seen from Table 4-2, no significant excitation of nickel fluorescence results when cobalt excitation is used and conversely, no significant fluorescence of cobalt is seen with nickel excitation. Also, Figure 4-8 shows the simplified fluorescence spectra obtained with a monochromator spectral bandpass of 1 nm.

Noise Considerations and Scatter Interferences

In order to determine the principle source of noise in this technique and to see if scattered radiation from the source ICP was present, a noise study was carried out for zinc at 213.9 nm and sodium at 589.0 nm in order to obtain an estimate of noise in the ultraviolet and visible regions of the spectrum.

The analytical precision (4s lock-in time constant, 10s integration time, using 16 consecutive readings) for the measurement of high concentration solutions was on the order of 2% for zinc and 10% for sodium and was limited to some extent by the source ICP stability. Other researchers (39, 68) have reported the ICP precision to be limited by the fluctuations in sample transport and nebulization to about 1%. The long-term stability of the ICP provides an advantage over other sources used for AFS such as electrodeless discharge lamps, which must be carefully thermostated (69) and the Eimac short-arc xenon lamp (70) which has a lower intensity in the ultraviolet. Also, there was no significant difference in the precision when the measurements for zinc and sodium were carried out in a matrix containing 10 mg mL^{-1} calcium. However, there was an increase in scattered radiation.

The precision for the measurement of low concentration solutions was about 3-4 times worse than that

for high concentration solutions. The scatter signal due to the calcium matrix at the zinc and sodium lines resulted in a 2-5 times increase in signal over the blank level, respectively. Even though scatter was observed due to the calcium matrix, it did not act as a significant noise source (precision for the low concentration measurements is about the same with and without the 10 mg mL^{-1} calcium matrix). Consequently, if present, scatter can be subtracted out by using the two-line technique (66), assuming that the scatter level does not change appreciably in the vicinity of the atomic fluorescence line.

Conclusions

While the fluorescence detection system is well-optimized for a background shot-noise limited system, the optical transfer of radiation from the source ICP to the atomization ICP could be improved by at least an order of magnitude through the use of an ellipsoidal reflector (71, 72) placed behind the plasma to collect a much larger solid angle of emission. Indeed, based upon solid angle considerations, less than 1% of the source radiation is presently being collected using 50 mm diameter lenses. Also, a mirror placed behind the atomization ICP in the direction of the fluorescence monochromator could be expected to improve detection

powers by two times and aspiration of higher concentration excitation solutions could also be used to increase the source intensity in some cases. However, clogging of the nebulizer and aerosol tube of the torch may result, as was noticed in this work for aluminum and sodium. The use of demountable torches with large diameter aerosol tubes might improve the situation.

Demers (73) has shown that for the HCL-ICP-AFS system (Baird Corp., Bedford, MA) the introduction of propane into the ICP has improved detection powers for the refractory elements. It could be expected, then, that the detection powers for ICP-ICP-AFS may be improved by the introduction of propane into the atomization ICP.

Table 4-1. Detection Limits for ICP-ICP-AFS and ICP-flame-AFS.

Species	Wavelength (nm)	ICP-ICP-AFS LOD (nm mL^{-1})[1]	ICP-flame-AFS[2] LOD (ng mL^{-1})
Al(I)	309.271	8000	1000
Ca(I)	422.673	60	4
Ca(II)	393.366	2	
Co(I)	240.725	100	11
Co(II)	228.616	300	
Cr(I)	357.869	900	2
Cr(II)	205.552	2000	
Cu(I)	324.754	30	2
Fe(I)	248.327	200	6
Fe(II)	259.940	100	
Mn(I)	279.827	70	2
Mn(II)	257.610	1	
Mo(I)	386.411	1000	
Mo(II)	202.030	20,000	
Na(I)	588.995	100	
Nd(II)	430.358	N.D.[3]	
Ni(I)	232.003	100	
Ni(II)	231.604	100	
Sm(II)	363.429	30,000	
Tb(II)	350.917	N.D.[3]	
V(I)	318.398	8000	400
V(II)	309.311	1000	
Yb(I)	398.799	100	
Yb(II)	369.419	200	
Zn(I)	213.856	4	0.5
Zn(II)	206.200	600	

[1]Limit of detection.

[2]Reported by Epstein *et al.* (7).

[3]Not detectable.

Table 4-2. Spectral Interferences for ICP-ICP-AFS

Mixture	Species/ Concentration in Source ICP	Species/ Concentration in Atomization ICP	Wavelength of Fluorescence Measured (nm)	Fluorescence Intensity (relative)
Zn-Cu	Zn/20 mg mL^{-1}	Cu/5000 µg mL^{-1}	213.9	0.30
		Zn/10 µg mL^{-1} + Cu/5000 µg mL^{-1}		100
Yb-Sm	Yb/20 mg mL^{-1}	Yb/100 µg mL^{-1}	369.4	100
		Sm/1000 µg mL^{-1}		1.3
		Yb/100 µg mL^{-1} + Sm/1000 µg mL^{-1}		98
Ni-Co	Co/20 mg mL^{-1}	Co/1000 µg mL^{-1}	231.2*	100
		Ni/1000 µg mL^{-1}		4.5
		Co/1000 µg mL^{-1} + Ni/1000 µg mL^{-1}		99
	Ni/20 mg mL^{-1}	Ni/1000 µg mL^{-1}	231.2	100
		Co/1000 µg mL^{-1}		2.0
		Ni/1000 µg mL^{-1} + Co/1000 µg mL^{-1}		97

*Taken on a 10 times more sensitive scale than Ni.

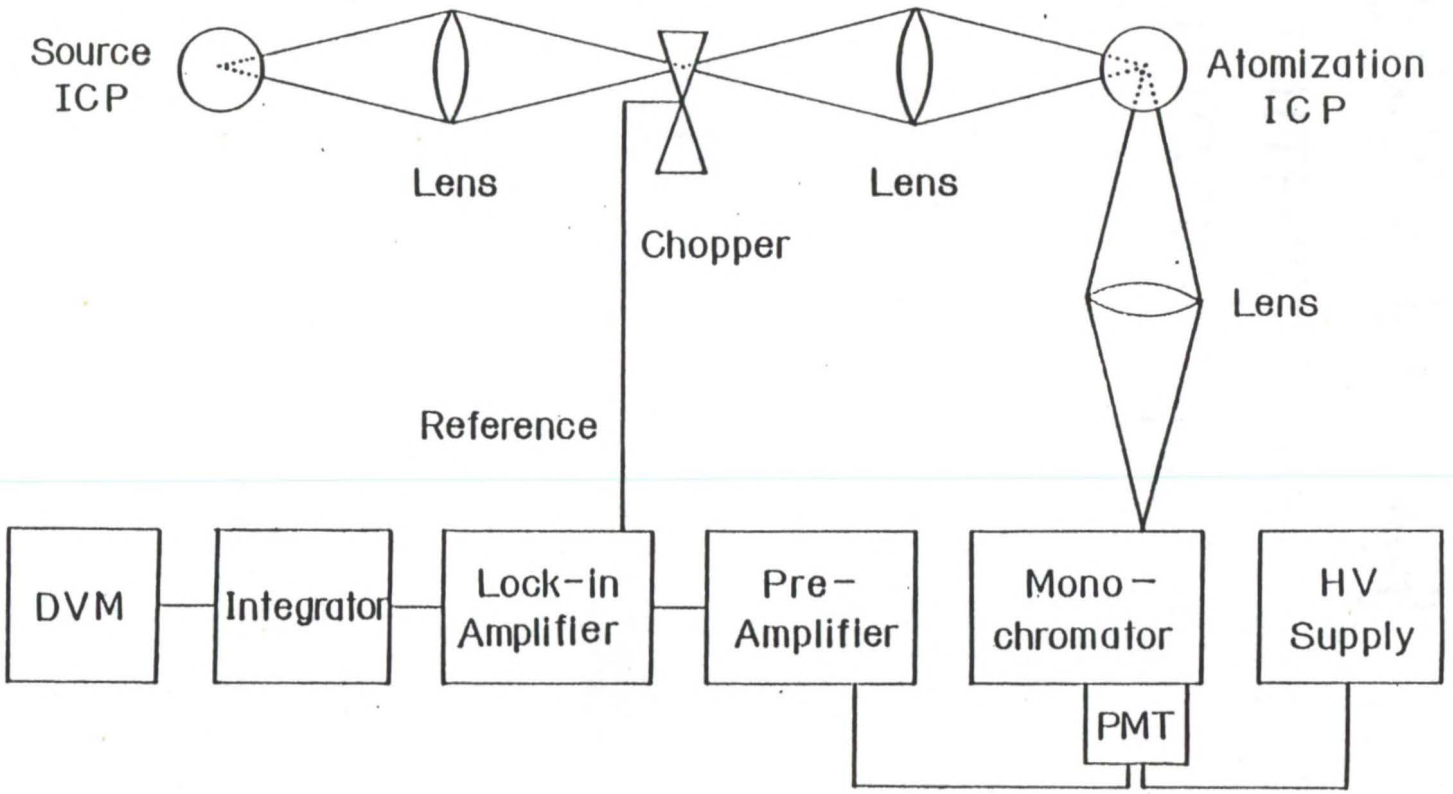

Figure 4-1. Block diagram of ICP-ICP-AFS system.

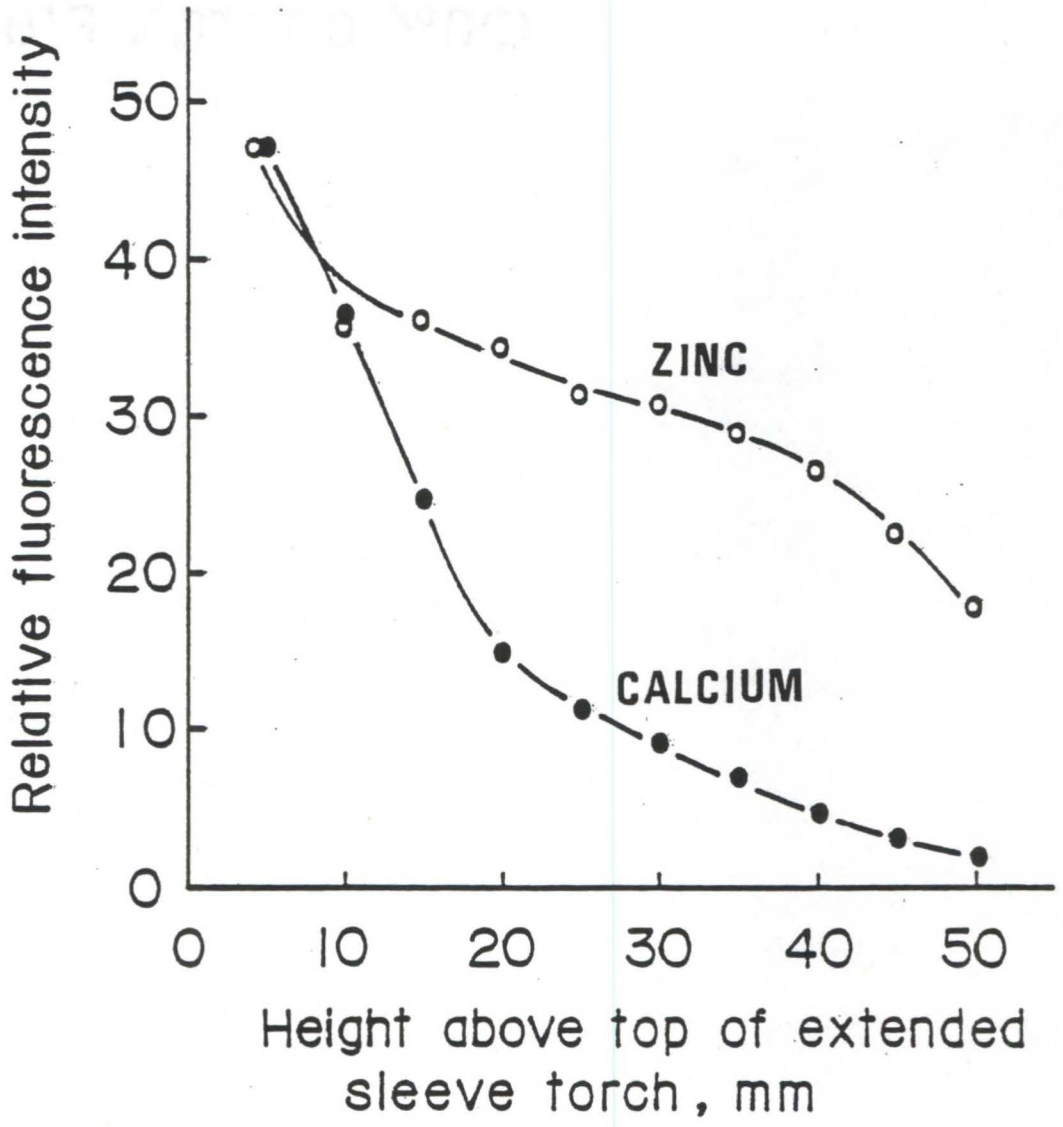

Figure 4-2. Vertical distributions of fluorescence intensities for zinc and calcium. RF powers: 2.0 kW source ICP 0.7 kW (Zn) and 1.0 kW (Ca) atomization ICP.

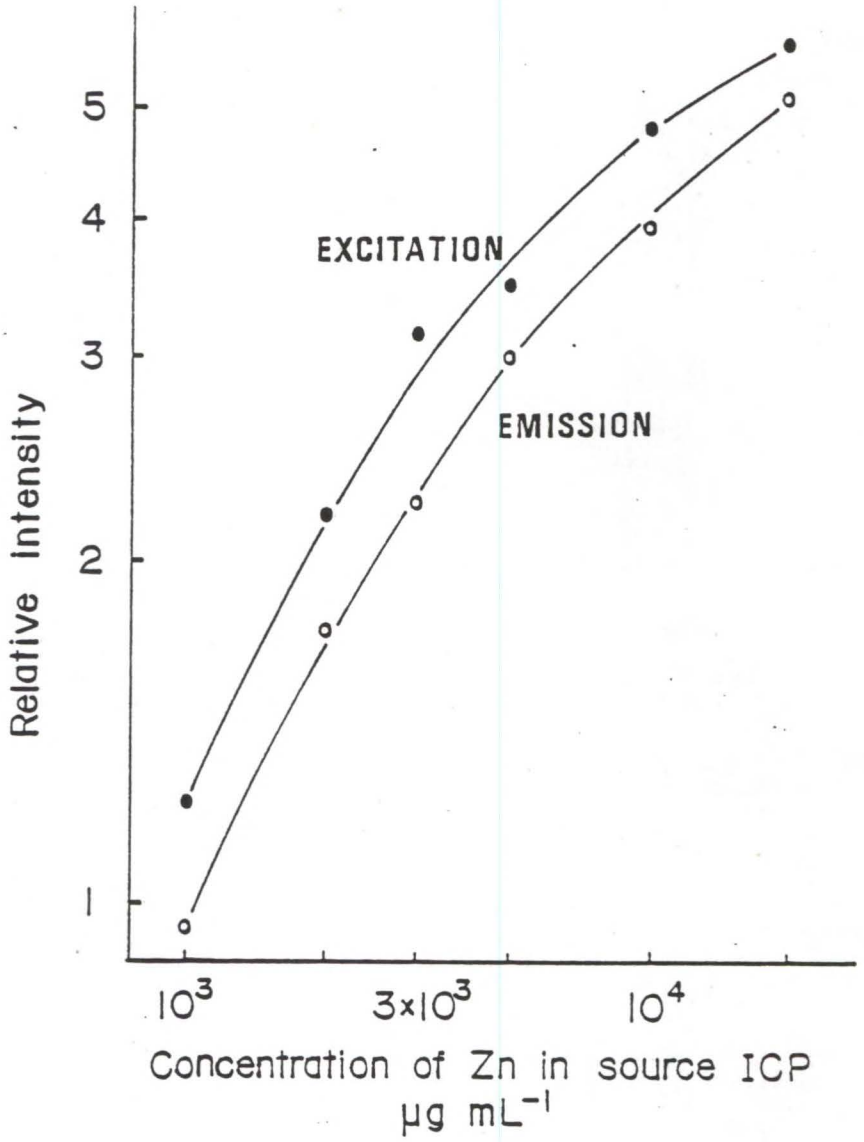

Figure 4-3. Excitation and emission curves of growth for zinc atom at 213.9 nm. Observation height: 40 mm above the top of the extended-sleeve torch for excitation (80 mm above the load coil); 20 mm above the load coil using the conventional short torch for emission; 1 μg/mL zinc aspirated into atomization ICP. RF powers: 2.0 kW source ICP, 0.7 kW atomization ICP.

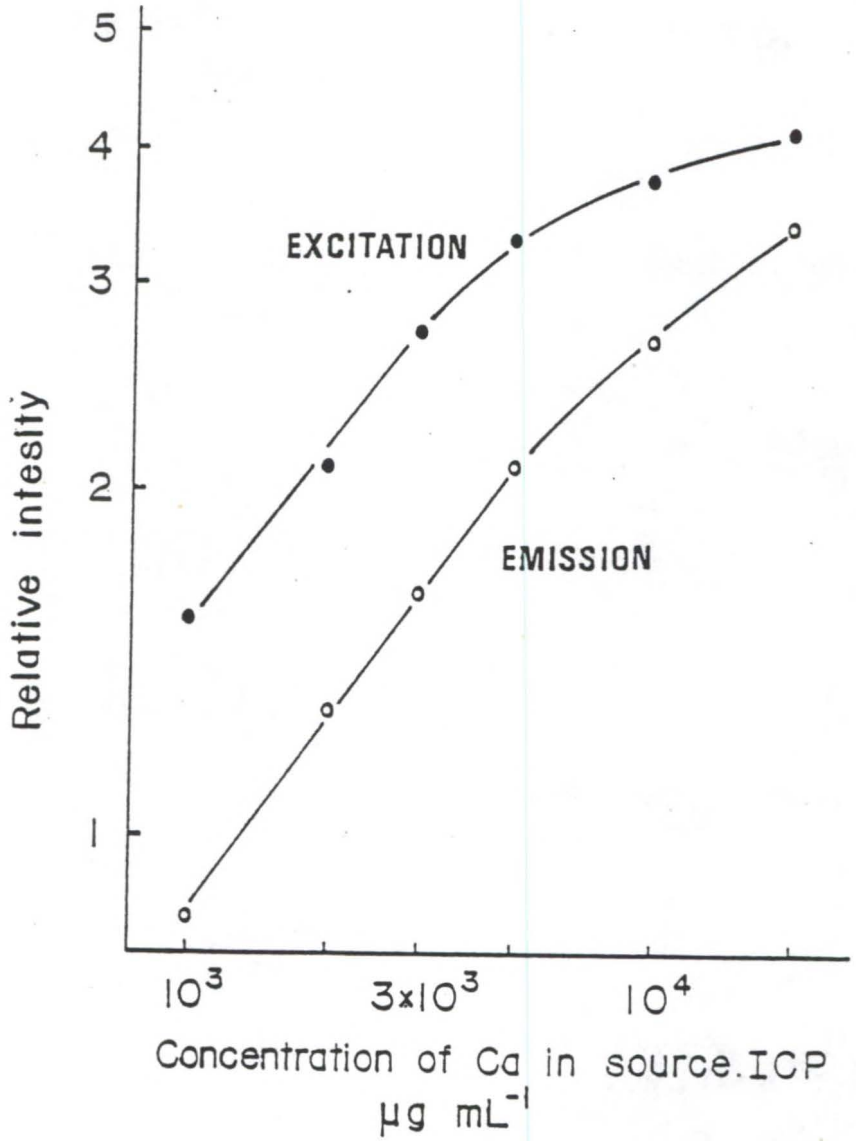

Figure 4-4. Excitation and emission curves of growth for calcium ion at 393.4 nm. Observation height: 20 mm above the top of the extended-sleeve torch for excitation (60 mm above the load coil); 20 mm above the load coil using the conventional short torch for emission; 1 μg/mL calcium aspirated into atomization ICP. RF powers: 2.0 kW source ICP, 0.7 kW atomization ICP.

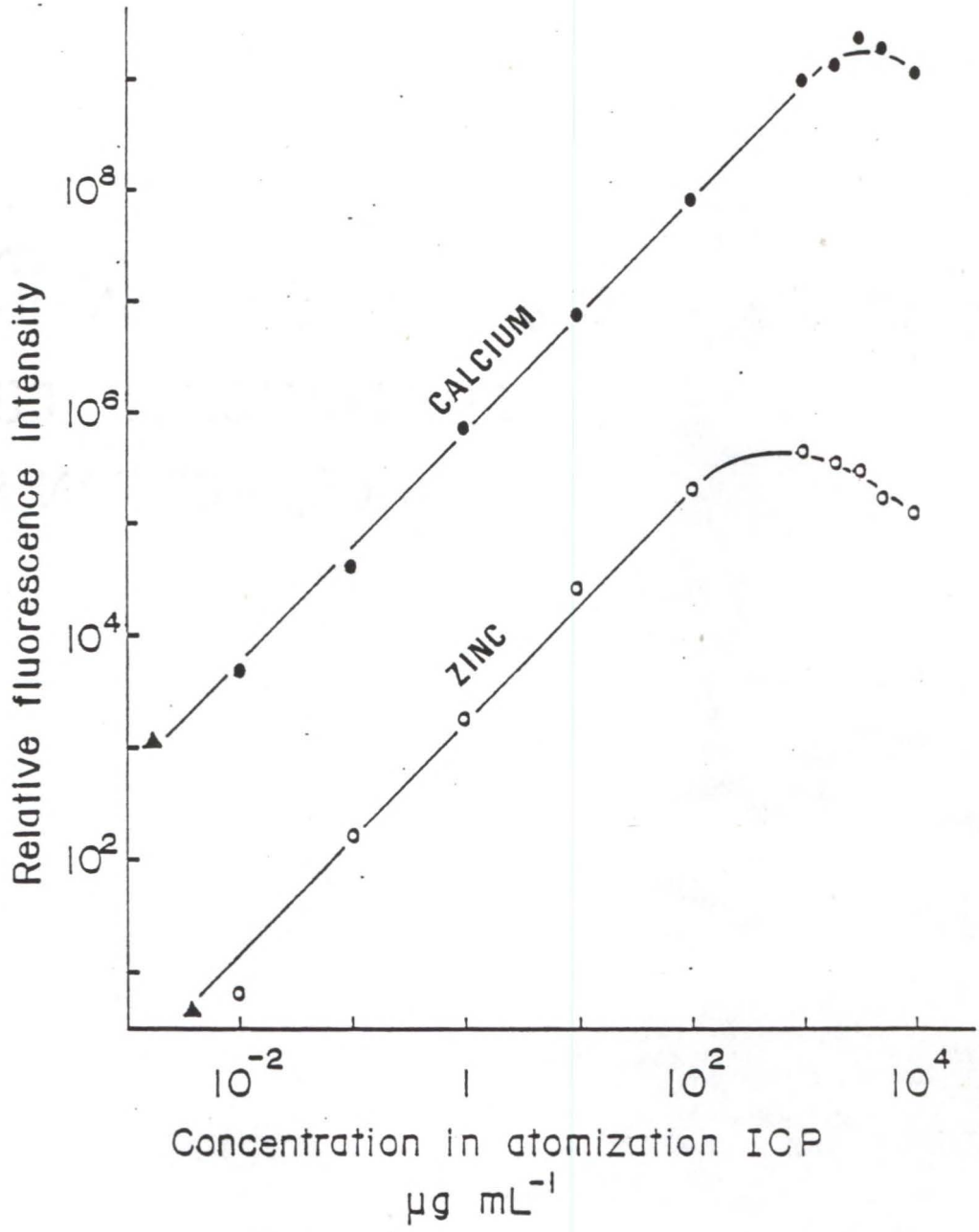

Figure 4-5. Analytical curves of growth for calcium and zinc. Observation height: 20 mm (Ca) and 40 mm (Zn) above the top of the extended-sleeve torch (60 mm and 80 mm above the load coil, respectively); 20 mg/mL analyte aspirated into source ICP. RF powers: 2.0 kW source ICP, 1.0 kW (Ca) and 0.7 kW (Zn) atomization ICP.

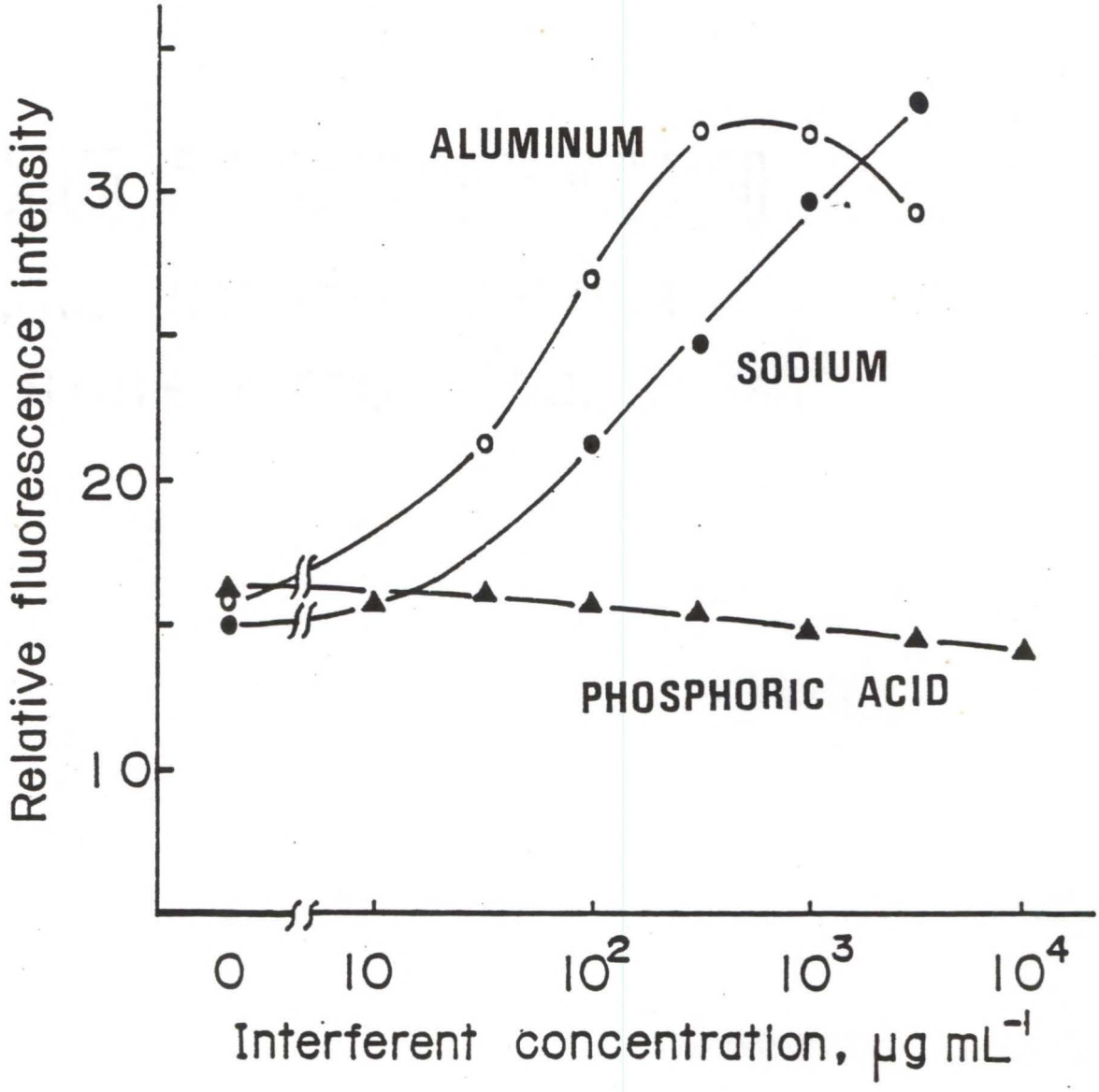

Figure 4-6. Effect of coexisting aluminum, sodium and phosphorus on resonance fluorescence intensities for calcium ion at 393.4 nm. Observation height: 20 mm above the top of the extended-sleeve torch (60 mm above the load coil). RF powers: 2.0 kW source ICP, 1.0 kW atomization ICP.

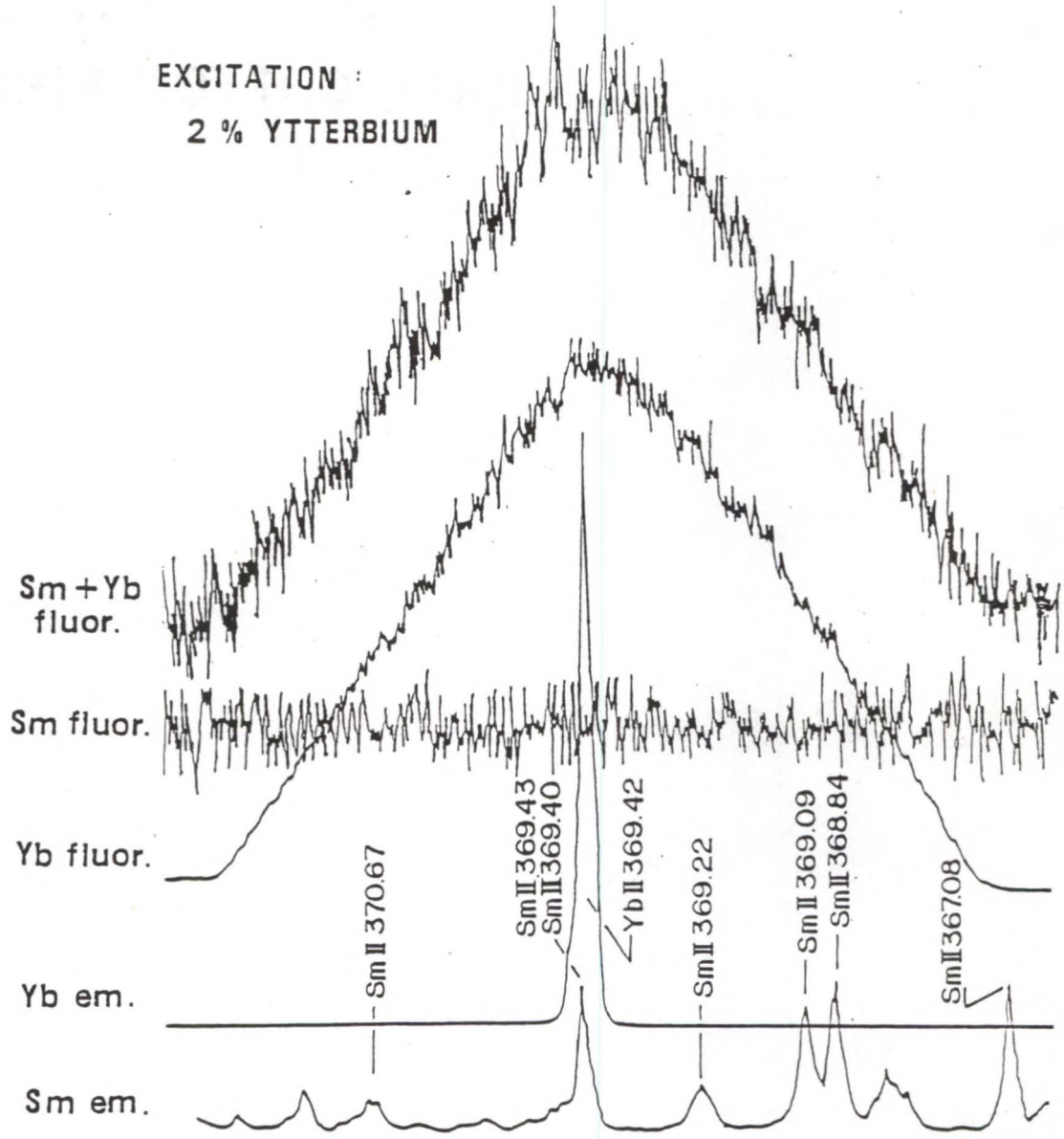

Figure 4-7. Fluorescence and emission spectra for 100 µg/mL ytterbium and 1000 µg/mL samarium. Observation height: 20 mm above the top of the extended-sleeve torch (60 mm above the load coil). RF powers: 2.0 kW source ICP, 1.0 kW atomization ICP. Spectral bandpass: 2 nm (fluorescence), 0.04 nm (emission).

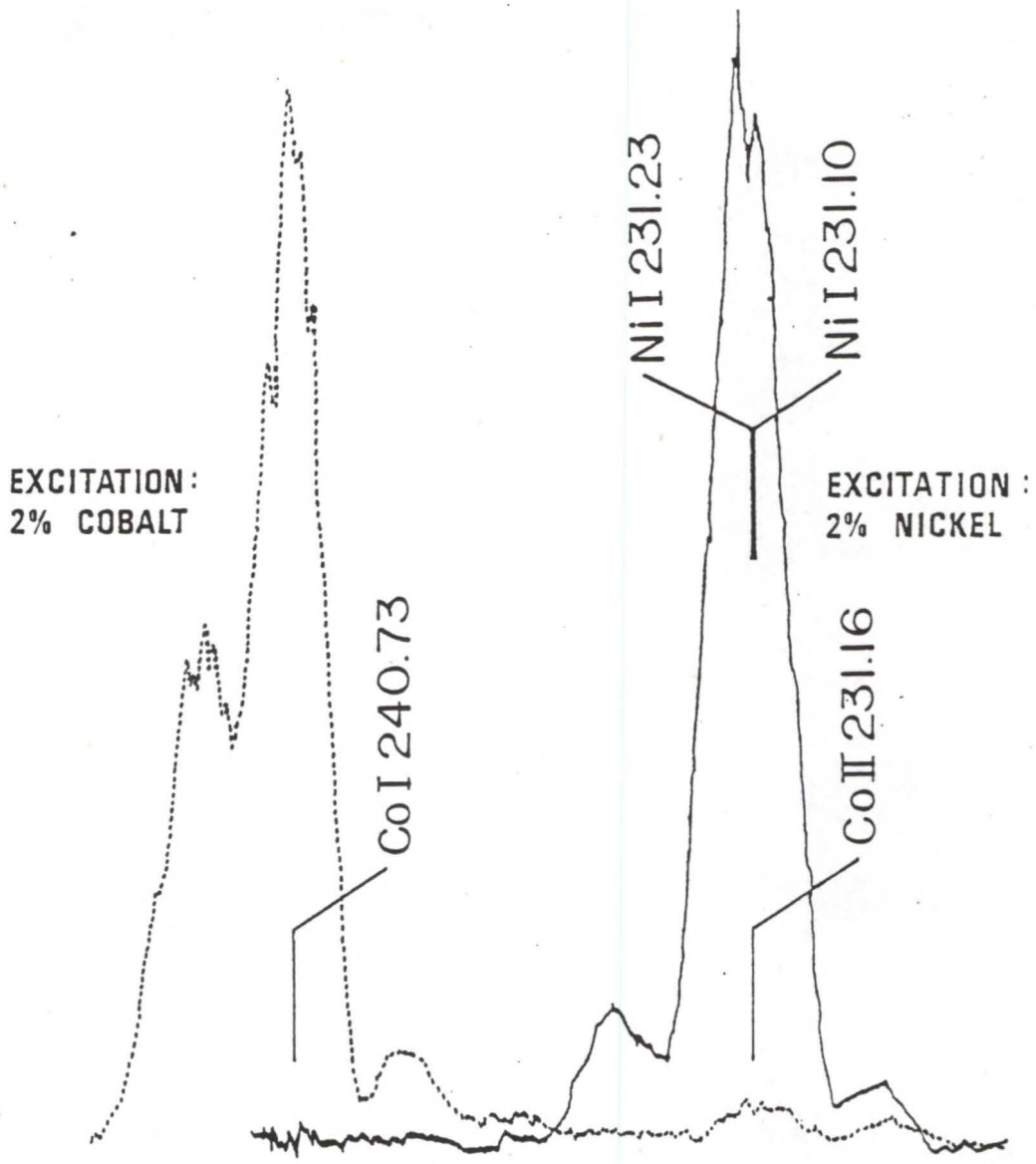

Figure 4-8. Fluorescence spectra for a 1000 µg/mL cobalt-1000 µg/mL nickel solution. Observation height: 40 mm above the top of the extended-sleeve torch (80 mm above the load coil). RF powers: 2.0 kW source ICP, 0.7 kW atomization ICP. Spectral bandpass: 1 nm.

CHAPTER V
FINAL COMMENTS AND SUMMARY

At the outset of this work, some specific objectives were outlined. A summary of the results obtained and conclusions reached will be given in this chapter.

For the laser-excited ICP-AFS technique, the principle factor affecting the fluorescence sensitivity seems to be the spontaneous transition probability (Einstein coefficient of spontaneous emission) value of the fluorescence line. The second factor appears to be the energy difference of the upper levels between the laser-excited and fluorescence lines. The maximum value of the energy difference for which thermally-assisted fluorescence can be observed is about 1.2 eV even if the spontaneous transition probability of the thermally-assisted level is high. A plot of the redistribution of thermally-assisted fluorescence for yttrium using laser excitation at 383.288 nm does not follow a Boltzmann distribution. The radiatively-excited level is overpopulated, and the other levels do not follow a Boltzmannian distribution with a reasonable temperature for the negative slope points. Consequently, the technique of thermally-assisted fluorescence is not well-suited for temperature measurements in the ICP. The RF power has a

significant effect on the fluorescence intensities observed and the excitation temperatures of the plasma. In general, atomic lines of non-refractory elements are best observed at low RF powers (~ 0.7 kW), ionic lines of non-refractory species and atomic lines of refractory species at approximately 1.0 kW and lines of species which exhibit excited-state fluorescence at powers of $\gtrsim$ 1.2 kW. High carrier argon flow rates (~ 1.2 L min^{-1}) should be used for fluorescence excited from the ground-state, since this will increase the analyte transport rate into the plasma and also decrease the plasma temperature. With a decrease in plasma temperature, an increase in the ground-state population can be achieved and consequently, an increase in fluorescence signals. For excited-state fluorescence, a lower carrier argon flow rate (~ 0.9 L min^{-1}) should be used in order to avoid decreasing the temperature of the plasma and thus, depopulating the excited-state level from which laser excitation occurs. The temperature of the plasma using an extended-sleeve torch is approximately 1000-1500K less than the temperature obtainable with a conventional short torch, and varies from ~ 3000-3800K depending on the RF power and observation height. Chemical interferences, such as refractory compound formation, aerosol ionic redistribution effects and ionization interferences do exist in the ICP. It is therefore necessary to optimize carefully the RF power and carrier

argon flow rate to minimize these effects. On the other hand, spectral interferences are not present in the laser-excited ICP-AFS technique. The ICP is a high quantum efficiency atomization/ionization cell. The extended-sleeve torch exhibits resistance to quenching by air entrainment in the plasma up to a height of approximately 40 mm above the top of the torch (80 mm above the load coil). Conversely, the quantum efficiency using a conventional short torch drops off rapidly with increase in observation height due to air entrainment. The quantum efficiency for a particular species is also dependent on the number of energy levels near the laser-excited level. In general, the more energy levels near the laser-excited level, the shorter the lifetime and smaller the quantum efficiency, due to collisional mixing of the levels near the radiatively-excited level. The extended-sleeve torch should be utilized for all fluorescence lines except excited-state fluorescence, due to the resistance of quenching by air entrainment and lower background emission. On the other hand, the conventional short torch should be utilized for excited-state fluorescence owing to the higher temperature obtainable with this torch. The optimal observation region in the plasma for excited-state fluorescence using the short torch is located 10 mm above the load coil while for all other lines, an observation height of 10 mm above the top of the extended-sleeve torch (50 mm above the load coil)

should be used. An expanded dye laser beam (~ 10 mm diameter) is also beneficial for increasing fluorescence signal intensities.

The ICP is useful as an excitation source for AFS studies and can be adapted for multielement analysis. For the ICP-ICP-AFS technique, the optimal observation region in the atomization ICP for atomic lines of non-refractory elements is located 40 mm above the top of the extended-sleeve torch (80 mm above the load coil) while that for all other lines is 20 mm above the top of the torch (60 mm above the load coil). The detection powers are suitable for trace element analysis without spectral interference. Aerosol ionic redistribution effects are observed for calcium fluorescence in the presence of sodium and aluminum. Consequently, the RF power and carrier argon flow rate must be optimized carefully to minimize these effects. The analytical precision for the ICP-ICP-AFS technique is limited to some extent by the source ICP stability, and scatter due to a high concentration calcium matrix is not a significant noise source. Clogging of the nebulizer and aerosol tube of the torch in the source ICP occurs in some cases using 2% excitation solutions. The use of a demountable torch with a large diameter aerosol tube might improve the situation. Lastly, the collection of a larger solid angle of emission from the source ICP, the placement of a mirror behind the atomization

ICP in the direction of the fluorescence monochromator and the introduction of propane into the plasma to obtain a reducing atmosphere and decrease formation of oxides, could be expected to improve the detection powers.

REFERENCES

1. V.A. Fassel and R.N. Kniseley, Anal. Chem., 46 1110A (1974).

2. S. Greenfield, H.M. McGeachin, and P.B. Smith, Anal. Chim. Acta, 84, 76 (1967).

3. H. Uchida and H. Matsui, Bunko Kenkyu, 27, 110 (1978).

4. D.R. Demers, Appl. Spectrosc., 22, 797 (1968).

5. J.M. Mansfield, Jr., M.P. Bratzel, Jr., H.O. Norgordon, D.O. Knapp, K.E. Zacha, and J.D. Winefordner, Spectrochim. Acta, 23B, 389 (1968).

6. R.M. Lowe, Spectrochim. Acta, 26B, 201 (1971).

7. M.S. Epstein, S. Nikdel, N. Omenetto, R. Reeves, J. Bradshaw, and J.D. Winefordner, Anal. Chem., 51, 2071 (1979).

8. L.M. Fraser and J.D. Winefordner, Anal. Chem., 50, 360 (1978).

9. S. Weeks, H. Haraguchi, and J.D. Winefordner, Anal. Chem., 50, 360 (1978).

10. D.J. Kalnicky, R.N. Kniseley, and V.A. Fassel, Appl. Spectrosc., 31, 137, (1977).

11. N. Omenetto and J.D. Winefordner, Prog. Anal. Atom. Spectry., 2, (1, 2) 1979.

12. N. Omenetto, S. Nikdel, R.D. Reeves, J.D. Bradshaw, J.N. Bower, and J.D. Winefordner, Spectrochim. Acta, 35B, 507 (1980).

13. N.S. Ham and P. Hannaford, J. Phys. B., 12, L199 (1979).

14. R.E. Russo and G.M. Heiftje, Appl. Spectrosc., 36, 92 (1982).

15. G. Zizak, J.D. Bradshaw, and J.D. Winefordner, Appl. Spectrosc, 35, 59 (1981).

16. J.D. Bradshaw, N. Omenetto, G. Zizak, J.N. Bower, and J.D. Winefordner, Appl. Opt., 19, 2709 (1980).

17. H. Haraguchi and J.D. Winefordner, Appl. Spectrosc., 31, 195 (1977).

18. H. Haraguchi and J.D. Winefordner, Appl. Spectrosc., 31, 330 (1977).

19. N. Omenetto, P. Benetti, and G. Rossi, Spectrochim. Acta, 27B, 453 (1972).

20. H. Haraguchi, B. Smith, S. Weeks, D.J. Johnson, and J.D. Winefordner, Appl. Spectrosc., 31, 156 (1977).

21. N. Omenetto, R.F. Browner, J.D. Winefordner, G. Rossi, and P. Benetti, Anal. Chem., 44, 1683 (1972).

22. P. Hannaford, Proceedings of the CSI, Cambridge, 1979.

23. D.S. Gough, P. Hannaford, and R.M. Lowe, Phys. Lett., in press.

24. D.S. Gough, P. Hannaford, and R.M. Lowe, J. Phys. B., in press.

25. A.P. Thorne, "Spectrophysics," Chapman and Hall, London, 1974.

26. N. Omenetto, M.S. Epstein, J.D. Bradshaw, S. Bayer, J.J. Horvath, and J.D. Winefordner, J. Quant. Spectrosc. Radiat., Transfer, 22, 287 (1979).

27. L.M. Fraser and J.D. Winefordner, Anal. Chem., 44, 1444 (1972).

28. B.D. Pollard, M.B. Blackburn, S. Nikdel, A. Massoumi, and J.D. Winefordner, Appl. Spectrosc., 33, 5 (1979).

29. M.S. Epstein, S. Nikdel., J.D. Bradshaw, M.A. Kosinski, J.N. Bower, and J.D. Winefordner, Anal. Chem. Acta, 113, 221 (1980).

30. C.H. Corliss and W.R. Bozman, NBS Monograph, 53 (1962).

31. P.W.J.M. Boumans, "Line Coincidence Tables for Inductively Coupled Plasma Atomic Emission Spectrometry," Pergamon Press, 1980.

32. N.O. Omenetto and J.D. Winefordner, Appl. Spectrosc, 26, 555 (1972).

33. H. Uchida, Spectrosc. Lett., 14, 655 (1981).

34. J. Jarosz, J.M. Mermet, and J.P. Robin, Spectrochim. Acta, 33B, 55 (1978).

35. G. Zizak, J.J. Horvath, C.A. van Dijk, and J.D. Winefordner, J. Quant. Spectrosc. Radiat. Transfer, 25, 525 (1981).

36. J.M. Mermet, Spectrochim. Acta, 30B, 383 (1975).

37. G.R. Kornblum and L. de Galan, Spectrochim. Acta, 29B, 249 (1974).

38. G.R. Kornblum and L. de Galan, Spectrochim. Acta, 32B, 71 (1977).

39. P.W.J.M. Boumans and F.J. de Boer, Spectrochim. Acta, 32B, 365 (1977).

40. H. Uchida, J. Ranabe, Y. Nojiri, H. Haraguchi, and K. Fuwa, Spectrochim. Acta, 36B, 711 (1981).

41. Y. Nojiri, K. Tanabe, H. Uchida, H. Haraguchi, K. Fuwa, and J.D. Winefordner, Spectrochim. Acta, submitted.

42. S. Murayama, Spectrochim. Acta, 25B, 191 (1970).

43. L.M. Fraser and J.D. Winefordner, Anal. Chem., 43, 1693 (1971).

44. J.Z. Kose, Phys. Review A, 19, 678 (1979).

45. C. Th. J. Alkemade, Rj. Hollander, W. Snelleman, and P.J. Th. Zeeger, "Metal Vapors in Flames," Pergamon Press (1982).

46. P.W.J.M. Boumans, Spectrochim. Acta, 37B, 75 (1982).

47. M.B. Denton and H.V. Malmstadt, Appl. Phys. Lett., 18, 485 (1971).

48. N. Omenetto, N.N. Hatch, L.M. Fraser, and J.D. Winefordner, Anal. Chem., 45, 195 (1973).

49. N. Omenetto, N.N. Hatch, L.M. Fraser, and J.D. Winefordner, Spectrochim. Acta, 28B, 65 (1973).

50. N. Omenetto, L.P. Hart, P. Benetti, and J.D. Winefordner, Spectrochim. Acta, 28B, 301 (1973).

51. N. Omenetto, P. Benetti, L.P. Hart, J.D. Winefordner, and C. Th. J. Alkemade, Spectrochim. Acta, 28B, 289 (1973).

52. A. Montaser and V.A. Fassel, Anal. Chem., 48, 1470 (1976).

53. D.R. Demers and C.D. Allemand, Anal. Chem., 53, 1915 (1981).

54. D.R. Demers, D.A. Busch, and C.D. Allemand, Amer. Lab., March, 167 (1982).

55. V. Sychra, V. Svoboda, and I. Rubeska, "Atomic Fluorescence Spectroscopy," Van Nostrand-Reinhold, New York (1975).

56. J.D. Winefordner, S.G. Schulman, and T.C. O'Haver, "Luminescence Spectrometry in Analytical Chemistry," in Chemical Analysis, Vol. 38, P.J. Elving and J.D. Winefordner, Eds., Wiley, New York (1972).

57. M. Hercher, Appl. Opt., 6, 947 (1967).

58. L. Huff and L.G. DeShazer, J. Opt. Soc. Amer., 60, 157 (1970).

59. E.H. Pepmeier, Spectrochim. Acta, 27B, 431 (1972).

60. E.H. Pepmeier, Spectrochim. Acta, 27B, 445 (1972).

61. N. Omenetto and J.D. Winefordner, "Atomic Fluorescence Spectroscopy with Laser Excitation," in Analytical Laser Spectroscopy, P.J. Elving and J.D. Winefordner, Eds., Wiley, New York (1979).

62. P.W.J.M. Boumans and M. Bosveld, Spectrochim. Acta, 34B, 59 (1979).

63. R.M. Barnes, Crit. Rev. Anal. Chem., 7, 203 (1978).

64. Ch. A.M. Hussein and G. Nickless, paper presented to the 2nd ICAS, Sheffield, England, 1969.

65. N. Omenetto, S. Nikdel, J.D. Bradshaw, M.S. Epstein, R.D. Reeves, and J.D. Winefordner, Anal. Chem., 51, 1521 (1979).

66. P.L. Larkins and J.B. Willis, Spectrochim. Acta, 29B, 319 (1974).

67. A.T. Zander, T.C. O'Haver, and P.N. Keliher, Anal. Chem., 49 (939 (1977).

68. P.W.J.M. Boumans, "Inductively Coupled Plasmas: State-of-the-Art in Research and Routine Analysis," paper presented at the 20th CSI and 7th ICAS, Prague, Czechoslovakia, 1977.

69. R.F. Browner, B.M. Patel, T.H. Glenn, M.E. Rielta, and J.D. Winefordner, Spectrosc. Lett., 5, 311 (1972).

70. R.L. Cochran and G.M. Hieftje, Anal. Chem., 49, 2040 (1977).

71. M. Shull and J.D. Winefordner, Anal. Chem., 43, 799 (1971).

72. P. Benetti, N. Omenetto, and G. Rossi, Appl. Spectrosc., 24, 57 (1971).

73. D.R. Demers, Baird Corp. Bedford, MA, private communication, 1982.

APPENDIX
GLOSSARY OF ACRONYMS

AAS	atomic absorption spectrometry
AES	atomic emission spectrometry
AFS	atomic fluorescence spectrometry
EDL	electrodeless discharge lamp
FWHM	full width at half-maximum
HCL	hollow cathode lamp
ICP	inductively coupled plasma
LEAFS	laser-excited atomic fluorescence spectrometry
LOD	limit of detection
LTE	local thermodynamic equilibrium
RF	radio-frequency
SNR	signal-to-noise ratio
VAEI	vaporization, atomization, excitation, ionization

BIOGRAPHICAL SKETCH

Michael Anthony Kosinski was born in Peabody, Massachusetts, on October 23, 1956. He attended Bishop Fenwick High School in Peabody and graduated magna cum laude from Salem State College in Salem, Massachusetts, with a B.A. in chemistry in 1978. Since then, he has attended the University of Florida where he received his Ph.D. in analytical chemistry in 1982 under the direction of Dr. James D. Winefordner.

I certify that I have read this study and that in my opinion it conforms to acceptable standards of scholarly presentation and is fully adequate, in scope and quality, as a dissertation for the degree of Doctor of Philosophy.

James D. Winefordner, Chairman
Graduate Research Professor
of Chemistry

I certify that I have read this study and that in my opinion it conforms to acceptable standards of scholarly presentation and is fully adequate, in scope and quality, as a dissertation for the degree of Doctor of Philosophy.

John G. Dorsey
Assistant Professor of
Chemistry

I certify that I have read this study and that in my opinion it conforms to acceptable standards of scholarly presentation and is fully adequate, in scope and quality, as a dissertation for the degree of Doctor of Philosophy.

Hugh A. Moye
Professor of Food Science and
Human Nutrition

This dissertation was submitted to the Graduate Faculty of the Department of Chemistry in the College of Liberal Arts and Sciences and to the Graduate Council, and was accepted as partial fulfillment of the requirements for the degree of Doctor of Philosophy.

December, 1982

Dean for Graduate Studies
and Research